Non–linear programming numerical formulation to acquire limit self–standing conditions of circular masonry arches accounting for limited friction

Giuseppe COCCHETTI[1], **Egidio RIZZI**[2*]

[1] Department of Civil and Environmental Engineering, Politecnico di Milano
piazza L. da Vinci 32, 20133, Milano, Italy
e–mail: giuseppe.cocchetti@polimi.it

[2] Department of Engineering and Applied Sciences, School of Engineering, University of Bergamo
viale G. Marconi 5, 24044, Dalmine (BG), Italy
e–mail: egidio.rizzi@unibg.it

*Corresponding Author

Accepted: 19 October 2019

Short Bio-Sketches

Giuseppe COCCHETTI is currently Associate Professor of Structural and Materials Mechanics (Scienza delle Costruzioni) at Politecnico di Milano. At Politecnico di Milano, he graduated cum Laude in Civil (Structural) Engineering in 1993; got a Doctoral Degree in Structural Engineering in 1998; became assistant professor in 2000 and associate professor in 2005. He received the Habilitation as full professor in 2014. He spent some research periods abroad. He has authored about 135 publications, 45 of which on refereed international journals.

Egidio RIZZI has been committed as Professor of Mechanics of Solids and Structures (Scienza delle Costruzioni) at three Italian universities since 1995: Politecnico di Milano 1995–1998, Assistant Professor; Politecnico di Bari, Faculty of Engineering at Taranto 1998–2001, Associate Professor; Università degli studi di Bergamo, 2001 to present, Associate/Full Professor. He is currently appointed at UniBG, School of Engineering (Dalmine), as Full Professor, since 2006. He graduated cum Laude in Civil Engineering at Politecnico di Milano in 1990. He later acquired a MSc in Civil Engineering (CU-Boulder, USA, 1993) and a Doctoral Degree in Structural Engineering (Politecnico di Milano, 1995). He has had several international collaborations and spent various research periods abroad. He has gained a research expertise in Structural Engineering, specifically in the field of Mechanics of Solids and Structures, along diversified research areas. He has authored about 150 publications, nearly 70 of which on different refereed international journals.

Abstract. *The modern rational Limit Analysis (LA) of masonry arches typically takes off from classical three Heyman hypotheses, a main one of them assuming that sliding failure shall not occur, like linked to unbounded friction. This allows for the computation of the least thickness of circular masonry arches under self–weight (Couplet–Heyman problem) and of the associated purely rotational collapse mode, by different analytical and numerical approaches. The aim of this work is to further investigate the collapse of circular masonry arches in the presence of limited friction. Here, the normality of the flow rule may no longer apply and the whole LA analysis shall be revisited. A new computational methodology based on non–linear programming is set forward, toward investigating all possible collapse states, by jointly looking at admissible equilibrium configurations and associated kinematic compatibility, in the spirit of the "uniqueness" theorem of LA. Critical values of friction coefficient are highlighted, marking the transitions of the arising collapse modes, possibly involving sliding. Uniqueness of critical arch thickness is still revealed, for symmetric arches of variable opening, at any given supercritical friction coefficient allowing the arch to withstand, despite the visible role of friction in shifting the final appearance of the collapse mode.*

Keywords: *Computational Limit Analysis (LA); circular masonry arches; minimum thickness; collapse mechanisms; limited friction.*

1 INTRODUCTION

The structural analysis of masonry arches of various shapes has been recently regaining a further momentum, based on the rational founding developments in modern times by the pioneering works of Jacques Heyman [1–4]. Thereby, classical Limit Analysis (LA) of ductile structures has been remarkably transferred to the field of masonry constructions, within the following three main typical behavioral assumptions: (a) masonry has no tensile strength; (b) masonry has infinite compressive strength; (c) sliding failure does not occur (friction is high enough to prevent any sliding).

Within such a framework, classical problems as that of finding the critical condition of least thickness for a circular masonry arch under self–weight *(Couplet–Heyman problem)* have found further consistent solutions by different analytical and numerical methodologies. For instance, worthwhile to be mentioned shall be contributions [5–53]. Specifically, refs. [5–33] concern the general analysis of masonry arches, possibly in conjunction with the determination of the critical least–thickness condition and considering different issues, such as various arch shapes (e.g. pointed, oval, elliptical, etc…) and possible variable stereotomy of the arch blocks (differing from that of classical radial joints, as here analyzed). Moreover, refs. [34–43] particularly deal with the issue of finite friction, and its implications in the statics of masonry arches and the possible failure modes. About the various adopted modelization approaches, refs. [44–53] provide different techniques of analysis for the statics of masonry arches, mostly applying numerical approaches, some even rather similar to the computational LA approach here employed, which leads to a novel complementarity problem formulation and an original non–linear mathematical programming implementation.

Along such a line of research, from the present authors, also as a framing of the current investigation, a comprehensive account on the treatment of symmetric circular masonry arches, with a general angle of embrace at infinite friction, has been analytically and numerically derived in [16,17,19]. This has pointed out to the differences between typical outcomes in terms of the characteristics at incipient collapse, in the critical condition of least thickness (thickness to radius ratio, angular position of the inner hinge, non–dimensional horizontal thrust), for a purely rotational collapse mode. Specifically, differences to classical Heyman solution, in the hypothesis of uniform self–weight distribution along the geometrical centerline of the arch,

have been revealed, showing Heyman solution for the critical arch characteristics in the limit collapse state to correspond to the solution of a rather feasible *"first–order" (meaning linear) algebraic problem* (solution of a system of three linear equations in the arch's collapse characteristics) and to constitute a sort of approximation of the truly correct one, within such a hypothesis, which is actually based on the solution of a slightly more involved *"second–order" (meaning quadratic) algebraic problem* (solution of a system of three quadratic equations), with an increasing divergence at increasing arch opening, especially for over–complete semicircular (horseshoe) arches [17]. Also, consistency with former more general Milankovitch [9] solution accounting for the correct location of the center of gravity of each theoretical chunk of the arch was fully recovered, although leading to the analysis of an even more complicated *"third–order" (meaning cubic) algebraic problem* (solution of a system of three cubic equations), despite for the rather similar final results, thus leading to favour, still, the analysis within the hypothesis of a self–weight distribution along geometrical centerline, though with the correct settlement of the Couplet–Heyman problem (specifically the imposition of the tangency condition of the line of thrust at the intrados of the arch). Analytical details on all that are particularly and extensively discussed in [17], which constitutes a fundamental framing and a general reference, with literature review, for the present positioning and further scheduled endeavours on the role of finite friction.

All these previous analyses of such a specific flow of investigation were considering purely rotational collapse modes only, by relying on the role of (infinite) friction, according to third Heyman hypothesis (c) above. Further, in [18], the effect of reducing friction was initially analyzed, based on such previous outcomes, with first consistent results from available separate contributions among the literature referred to above, on top of the present discussion. In such a context, the issue arises about the possible effects of *non–normality of the flow rule* linked to rotation/sliding kinematics that may come up to spoil the typical implant of LA, as transferred from a classical framing of ductile structures (e.g. steel frames) to masonry ones, in Heyman sense [1–4]. Thus, the question arises whether more general formulations may be foreseen to investigate if non–normality may lead to non–unique collapse characteristics (as multiple load multipliers or, here, critical arch thicknesses). Along these lines, see for instance the various attempts in [44,53–57]. Despite that under specific conditions, like those related to arch symmetry and to simple loading (as self–weight only), non–normality effects may not arise in the outcomes of the collapse characteristics, neither at reducing friction (see e.g. [23,35,36]), a more general and consistent tool of analysis shall anyway be devised to investigate the link between non–normality (of the flow rule) and non–uniqueness (of critical arch thickness). A preliminary outline of the present developments has been presented in conference paper [20], with a main reference devoted to the full complete semicircular arch.

The present paper outlines a *general computational procedure of non–linear programming* apt to simultaneously enforce the condition of equilibrium and compatibility of a masonry arch at incipient collapse, as in the spirit of the "uniqueness" (or "mixed") theorem, and "direct" method, in the LA of ductile frames. Indeed, the "uniqueness" theorem of LA basically states that, for standard (i.e. associative) flow rules, if a "kinematic" (upper-bound) load multiplier is also a "static" (lower-bound) load multiplier, then it corresponds to the sought collapse load multiplier. In the context of non-associative flow rules, that would lead, though, to a potential range of collapse load multipliers, with non-uniqueness on it. The present handling is specifically referring to that, and seeking all collapse states that shall fulfill both static and kinematic requirements, thus attempting to inspect if any non-associative non-uniqueness may arise, due to limited friction. Thus, the formulation enforces at the same time equilibrium and compatibility, and numerically seeks all feasible states respecting that, at variable arch thickness and friction coefficient, as free varying parameters.

The computational procedure is implemented so far for circular masonry arches with any number of blocks (displaying radial joints) and opening angles, including for symmetrical or unsymmetrical instances of arch geometry, and leaving in principle the door open, for symmetric arches, to unsymmetrical solutions in terms of the deciphered collapse mechanisms (see e.g. Figures 12, 13 and 17, reported later in the body of results), since symmetry is not a priori imposed in the resulting collapse mode. The numerical procedure, starting from typical premises as those outlined in [58–62], and, in related, though different LA contexts for the treatment of 3D truss–frame ductile structures ([63–68]), minimizes an objective function that is linked to the complementarity relation between underlying static and kinematic variables. The procedure is shown to produce rather consistent results in terms of the collapse modes that may be encountered at a reducing friction coefficient among the blocks (purely rotational, mixed sliding–rotational, purely sliding, overturning), still revealing a uniqueness of the underlying solution in terms of critical arch thickness, despite for potential effects due to non–normality, at least in the quested context (symmetric circular arches under self–weight).

The structure of the paper goes as follows. Section 2 presents the general formulation and both kinematic and static descriptions. Section 3 outlines a selection of numerical results for symmetric under–complete, complete and over–complete circular masonry arches. Section 4 gathers a few conclusions from the achieved outcomes, outlining new scenarios of development for the analysis of circular masonry arches at limited friction.

2 GENERAL HYPOTHESES AND PROBLEM FORMULATION

Typical above–recalled Heyman hypotheses are thought to apply, except for the hypothesis of high friction, which is led to be reduced or, say, limited, to investigate the effect of possible sliding onsets and their development in the recorded collapse mode.

A circular masonry arch of mean radius r is considered (Figure 1), with a general angle of embrace, possibly unsymmetrically supported, i.e. with bisector line at half angle of embrace tilting to the vertical, and number of blocks (also apt to represent a continuous arch with the appropriate number of blocks, in the competent arising collapse mechanism). The number of blocks is labeled by integer n. Thickness t (thickness to radius ratio $\eta = t/r$) and friction coefficient μ are considered to be known, and are parametrically varied within the analyses. Stereotomy here considers radial joints only. Out–of–plane width is labeled d and self–weight per unit volume γ, so that self–weight per unit length, as distributed along the geometrical centerline of the arch, is $\gamma\, t\, d$.

The present formulation, and relative implementation, is rather general, as suggested by the morphology depicted in Figure 1, generally referring to unsymmetric circular arches. Despite, results in the paper would so far concern symmetric arches only (where uniqueness in critical arch thickness will still turn out to apply). Unsymmetric arches may subsequently be numerically analyzed elsewhere.

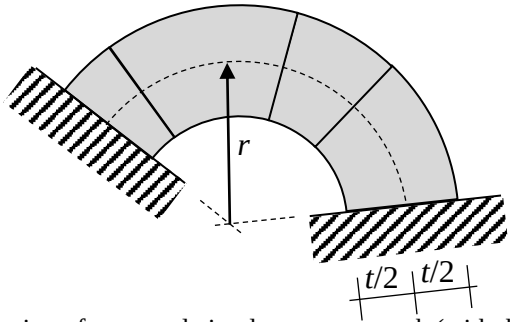

Figure 1: Geometric representation of a general circular masonry arch (with thickness to radius ratio $\eta = t/r$).

2.1 Kinematic and static description premises

About kinematics, only rigid–body movements avoiding compenetration between rigid adjacent blocks, with even a possible complete detachment, are admitted (see Figure 2), as discussed by the following kinematic description.

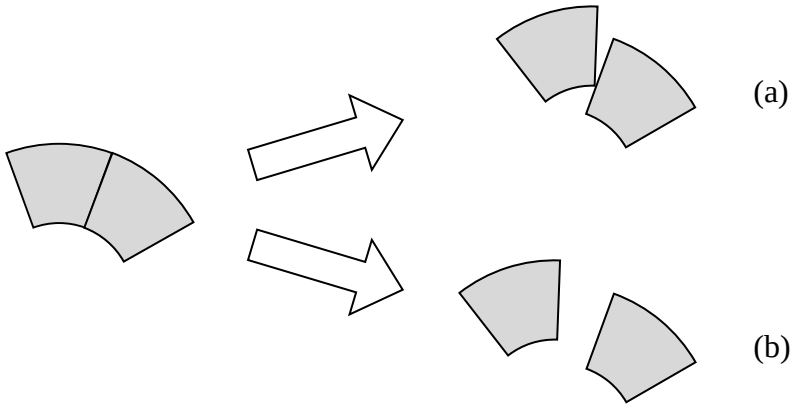

Figure 2: Admitted relative movements among adjacent rigid masonry blocks:
(a) rotation + sliding; (b) separation.

The four basic relative block movements depicted in Figure 3, all associated to non–negative kinematic variables, can be adopted by the superposition of effects to represent the relative motions above illustrated in Figure 2.

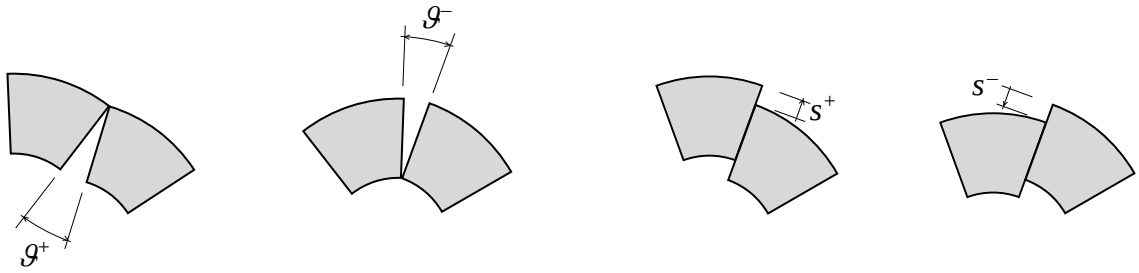

Figure 3: Kinematic description and variables of relative (rotational and sliding) movements among adjacent rigid masonry blocks.

About statics, the internal actions within the circular masonry arch can be defined by the assumptions shown in Figure 4.

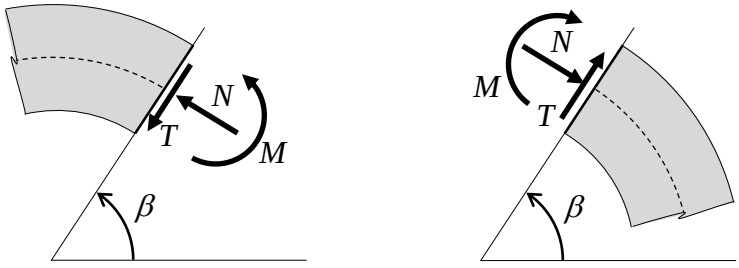

Figure 4: Assumptions of sign conventions for the internal actions within the circular arch.

Given Heyman constraint of no tensile strength, it is assumed that the arch can guarantee the equilibrium conditions only if resulting axial force N is applied within arch thickness t and if shear force T is limited by a Coulomb friction relationship, namely when:

$$\begin{cases} -N\frac{t}{2} \le M \le N\frac{t}{2} \\ -\mu N \le T \le \mu N \end{cases} \tag{1}$$

$\mu = \tan\phi$ being the friction coefficient of the generic joint of the masonry arch (and ϕ the relevant friction angle).
Relations (1) can be cast into the following equivalent form, by defining subsequent static *rotation and sliding activation functions* φ:

$$\begin{cases} \varphi_{\vartheta^+} = \quad M - N\frac{t}{2} \le 0 \\ \varphi_{\vartheta^-} = -M - N\frac{t}{2} \le 0 \\ \varphi_{s^+} = \quad T - \mu N \le 0 \\ \varphi_{s^-} = -T - \mu N \le 0 \end{cases} \tag{2}$$

Then, it can be observed that, starting from the initial geometrical configuration of the arch, an "orthogonality" [69] (product cancellation law) relation holds among each one of the four kinematic variables represented in Figure 3 (actually of their rates) and the corresponding activation function, i.e.:

$$\varphi_{\vartheta^+}\ \dot{\vartheta}^+ = 0, \quad \varphi_{\vartheta^-}\ \dot{\vartheta}^- = 0, \quad \varphi_{s^+}\ \dot{s}^+ = 0, \quad \varphi_{s^-}\ \dot{s}^- = 0 \tag{3}$$

Relations (3) and the sign constraints on the underlying variables then yield a system of *complementarity conditions* (see e.g. [61] and [69–73]), which represent the set of "*constitutive relations*" for the generic masonry joint:

$$\boldsymbol{\varphi} = \begin{bmatrix} \varphi_{\vartheta^+} = \quad M - N\frac{t}{2} \\ \varphi_{\vartheta^-} = -M - N\frac{t}{2} \\ \varphi_{s^+} = \quad T - \mu N \\ \varphi_{s^-} = -T - \mu N \end{bmatrix} \le \mathbf{0}, \qquad \dot{\boldsymbol{\lambda}} = \begin{bmatrix} \dot{\vartheta}^+ \\ \dot{\vartheta}^- \\ \dot{s}^+ \\ \dot{s}^- \end{bmatrix} \ge \mathbf{0}, \qquad \boldsymbol{\varphi}^T \dot{\boldsymbol{\lambda}} = 0 \tag{4}$$

2.1.1. Complete detachment and particular conditions

Toward discussing particular conditions that will arise in the following, the present section examines particular kinematic and static conditions that may occur, which are necessary for a complete *a priori* description of the solution classes and also for the interpretation of forthcoming numerical results that will arise.

It is worth noting that relations (4) directly include also a "*complete detachment*" condition, namely a total separation of two adjacent blocks, described by the contemporary activation of two independent and non–negative rotations ϑ^+ and ϑ^-, as shown in Figure 5.

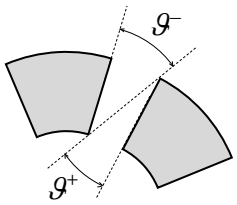

$$\begin{cases}\vartheta^+ > 0\\ \vartheta^- > 0\end{cases}$$

Figure 5: Possible complete separation of two adjacent masonry blocks at a common joint.

In such a block separation case, due to "orthogonality" conditions (3), the corresponding activation rotation functions must be zero:

$$\begin{cases}\varphi_{\vartheta^+} = \quad M - N\frac{t}{2} = 0\\ \varphi_{\vartheta^-} = -M - N\frac{t}{2} = 0\end{cases} \quad \Rightarrow \quad \begin{cases}N = 0\\ M = 0\end{cases} \tag{5}$$

which means a zero value for both axial force *N* and bending moment *M*. The remaining two inequalities, ruling sliding activation, reduce to the following ones:

$$\begin{cases}\varphi_{s^+} = \quad T - \mu N = \quad T \le 0\\ \varphi_{s^-} = -T - \mu N = -T \le 0\end{cases} \quad \Rightarrow \quad T = 0 \tag{6}$$

also implying a nil value for shear force *T* and a free relative tangential velocity $\dot{v}_s$:

$$\dot{v}_s = \dot{s}^+ - \dot{s}^-, \qquad \begin{cases}\dot{s}^+ \ge 0\\ \dot{s}^- \ge 0\end{cases} \tag{7}$$

Conversely, when it results that $N = 0$ at a masonry joint, four inequalities $(4)_a$ become:

$$\begin{cases}\varphi_{\vartheta^+} = \quad M \le 0\\ \varphi_{\vartheta^-} = -M \le 0\\ \varphi_{s^+} = \quad T \le 0\\ \varphi_{s^-} = -T \le 0\end{cases} \quad \Rightarrow \quad \begin{cases}M = 0\\ T = 0\end{cases} \quad \Rightarrow \quad \begin{cases}\varphi_{\vartheta^+} = 0\\ \varphi_{\vartheta^-} = 0\\ \varphi_{s^+} = 0\\ \varphi_{s^-} = 0\end{cases} \tag{8}$$

which, according to orthogonality conditions $(4)_c$, imply:

$$\dot{\boldsymbol{\lambda}} = \begin{bmatrix} \dot{\vartheta}^+ \\ \dot{\vartheta}^- \\ \dot{s}^+ \\ \dot{s}^- \end{bmatrix} \geq \mathbf{0} \tag{9}$$

namely, a possible complete detachment of the joint ($\dot{\vartheta}^+ > 0$ and $\dot{\vartheta}^- > 0$), with a possible free tangential velocity ($\dot{v}_s = \dot{s}^+ - \dot{s}^-,\ \dot{s}^+ \geq 0,\ \dot{s}^- \geq 0$).

It has to be underlined that when a compressive axial force acts at a masonry joint ($N > 0$), two sliding activation functions, φ_{s^+} and φ_{s^-}, cannot be both active together; as a consequence, also the two corresponding kinematic sliding variables cannot be both contemporarily active, i.e. they become "orthogonal" ($\dot{s}^+ \, \dot{s}^- = 0$).

However, in the quite specific case of a *nil axial force* ($N = 0$ and, then, $T = 0$ and $M = 0$), a multiplicity of mathematical optimum solutions can correspond to the same physical solution, being two sliding activation functions φ_{s^+} and φ_{s^-} both active (see Eq. (6)) and, consequently, two sliding variables $\dot{s}^+$ and $\dot{s}^-$ result to be undefined for the same (finite) value of $\dot{v}_s$ (Eq. (7)). Then, in order to eliminate such a multiplicity, a (weak) "orthogonality" condition among non–negative variables $\dot{s}^+$ and $\dot{s}^-$ can be added to the problem statement:

$$\dot{s}^+ \, \dot{s}^- = 0 \tag{10}$$

Finally, it is worth noting that the case of a *tensile* (i.e. strictly negative) *axial force* ($N < 0$) is *unfeasible* and it cannot constitute a solution to complementarity relations (4), being in this case:

$$\begin{cases} \varphi_{\vartheta^+} = \ \ M - N\frac{t}{2} \leq 0 \\ \varphi_{\vartheta^-} = -M - N\frac{t}{2} \leq 0 \\ \varphi_{s^+} = \ \ T - \mu N \leq 0 \\ \varphi_{s^-} = -T - \mu N \leq 0 \end{cases} \quad \Rightarrow \quad \begin{cases} M \leq N\frac{t}{2} < 0 \\ -M \leq N\frac{t}{2} < 0 \\ T \leq \mu N < 0 \\ -T \leq \mu N < 0 \end{cases} \tag{11}$$

Endly, it is worthwhile to mention that a case corresponding to Figure 2a does **not** require a dedicated treatment, since such a case automatically arises from the present general formulation.

2.2 Kinematic description of the arch

Being the arch composed of a set of rigid blocks, the kinematic description of the arch configuration reduces to the description of the rigid–body motion of each rigid block, limited by the excluded compenetration among the rigid blocks and by the given external kinematic constraint conditions.

For the k–th block, centroid G_k is chosen as a reference point for its rigid–body motion (such a choice is not only natural but also convenient for the later coupling with the forthcoming static analysis; moreover, this leaves the door open to set the self-weight distribution, in the static analysis, according to Milankovitch [9] or Heyman [1–4] hypotheses; in addition, it should be mentioned at this stage that, concerning the present pure kinematic analysis, the reference point could be any arbitrary point of the plane, possibly of the block, and such an assumption does not hinder the level of generality in any way); u and v are the horizontal and vertical displacements, respectively, of selected points of the block, in a Cartesian reference system (see Figure 6); ψ_k is the counter–clockwise rotation of the block.

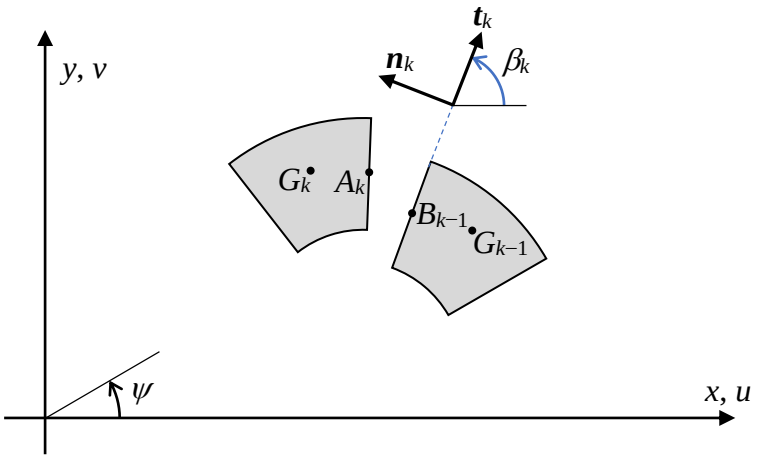

Figure 6: Specific points and variables for two generic adjacent masonry blocks in the current arch configuration (u, v and ψ mark horizontal and vertical displacements and counter–clockwise rotation, respectively).

The velocity at point A_k of the k–th block can be obtained by adding the relative velocities to the velocity at B_{k-1} of the (k–1)–th block, A_k and B_{k-1} being the points at half thickness (see Figure 6):

$$\dot{\boldsymbol{u}}_{A_k} = \dot{\boldsymbol{u}}_{B_{k-1}} + (\dot{s}_k^+ - \dot{s}_k^-)\,\boldsymbol{t}_k + \left(\dot{\vartheta}_k^+ + \dot{\vartheta}_k^-\right)\frac{t}{2}\boldsymbol{n}_k \tag{12}$$

where: $\boldsymbol{u} = [u, v]^T$; $\boldsymbol{n}_k$ and $\boldsymbol{t}_k$ being, respectively, the normal and tangential versors to the surface of the k–th joint (see Figure 6).

The velocities at A_k and B_{k-1} can be expressed, by rigid–body motions, as functions of the velocities at centroids G_k and G_{k-1}, respectively:

$$\dot{\boldsymbol{u}}_{A_k} = \dot{\boldsymbol{u}}_{G_k} + \begin{bmatrix} -\left(y_{A_k} - y_{G_k}\right) \\ \left(x_{A_k} - x_{G_k}\right) \end{bmatrix} \dot{\psi}_k \,, \quad \dot{\boldsymbol{u}}_{B_{k-1}} = \dot{\boldsymbol{u}}_{G_{k-1}} + \begin{bmatrix} -\left(y_{B_{k-1}} - y_{G_{k-1}}\right) \\ \left(x_{B_{k-1}} - x_{G_{k-1}}\right) \end{bmatrix} \dot{\psi}_{k-1} \tag{13}$$

By using rigid–body motion Eqs. (13) and the equation relating the angular velocities of the adjacent blocks, it results that:

$$\begin{cases} \dot{\boldsymbol{u}}_{G_k} = \dot{\boldsymbol{u}}_{G_{k-1}} + \begin{bmatrix} \left(y_{A_k} - y_{B_{k-1}}\right) - \left(y_{G_k} - y_{G_{k-1}}\right) \\ -\left(x_{A_k} - x_{B_{k-1}}\right) + \left(x_{G_k} - x_{G_{k-1}}\right) \end{bmatrix} \dot{\psi}_{k-1} + \\ \qquad\qquad - \begin{bmatrix} \left(y_{A_k} - y_{G_k}\right) \\ -\left(x_{A_k} - x_{G_k}\right) \end{bmatrix} \left(\dot{\vartheta}_k^+ - \dot{\vartheta}_k^-\right) + \left(\dot{s}_k^+ - \dot{s}_k^-\right) \boldsymbol{t}_k + \left(\dot{\vartheta}_k^+ + \dot{\vartheta}_k^-\right) \frac{t}{2} \boldsymbol{n}_k \\ \dot{\psi}_k = \dot{\psi}_{k-1} - \dot{\vartheta}_k^+ + \dot{\vartheta}_k^- \end{cases} \tag{14}$$

Finally, exploiting the initial geometry of the arch in the reference configuration, where radial joints of inclinations β_k converge to the center of the circle describing the circular geometric profile of the arch (the origin of the Cartesian system being set at that center):

$$\begin{cases} x_{A_k} = x_{B_{k-1}} = r \cos \beta_k \\ y_{A_k} = y_{B_{k-1}} = r \sin \beta_k \end{cases}, \qquad \boldsymbol{t}_k = \begin{bmatrix} \cos \beta_k \\ \sin \beta_k \end{bmatrix}, \qquad \boldsymbol{n}_k = \begin{bmatrix} -\sin \beta_k \\ \cos \beta_k \end{bmatrix} \tag{15}$$

it results that:

$$\begin{cases} \dot{u}_{G_k} = -\left[\left(r + \frac{t}{2}\right) \dot{\vartheta}_k^+ - \left(r - \frac{t}{2}\right) \dot{\vartheta}_k^-\right] \sin \beta_k + y_{G_k} \left(\dot{\vartheta}_k^+ - \dot{\vartheta}_k^-\right) + \\ \qquad\qquad + \left(\dot{s}_k^+ - \dot{s}_k^-\right) \cos \beta_k \; + \dot{u}_{G_{k-1}} - \left(y_{G_k} - y_{G_{k-1}}\right) \dot{\psi}_{k-1} \\ \dot{v}_{G_k} = +\left[\left(r + \frac{t}{2}\right) \dot{\vartheta}_k^+ - \left(r - \frac{t}{2}\right) \dot{\vartheta}_k^-\right] \cos \beta_k - x_{G_k} \left(\dot{\vartheta}_k^+ - \dot{\vartheta}_k^-\right) + \\ \qquad\qquad + \left(\dot{s}_k^+ - \dot{s}_k^-\right) \sin \beta_k + \dot{v}_{G_{k-1}} + \left(x_{G_k} - x_{G_{k-1}}\right) \dot{\psi}_{k-1} \\ \dot{\psi}_k = \dot{\psi}_{k-1} - \dot{\vartheta}_k^+ + \dot{\vartheta}_k^- \end{cases} \tag{16}$$

This set of recursive kinematic equations can be written for each of the n blocks of the arch ($k = 1,\ldots,n$). Specifically, for the first block ($k = 1$, $k–1 = 0$, being the fixed basement on the right) it results that:

$$\begin{cases} \dot{u}_{G_1} = -\left[\left(r + \frac{t}{2}\right) \dot{\vartheta}_1^+ - \left(r - \frac{t}{2}\right) \dot{\vartheta}_1^-\right] \sin \beta_1 + y_{G_1} \left(\dot{\vartheta}_1^+ - \dot{\vartheta}_1^-\right) + \left(\dot{s}_1^+ - \dot{s}_1^-\right) \cos \beta_1 \\ \dot{v}_{G_1} = +\left[\left(r + \frac{t}{2}\right) \dot{\vartheta}_1^+ - \left(r - \frac{t}{2}\right) \dot{\vartheta}_1^-\right] \cos \beta_1 - x_{G_1} \left(\dot{\vartheta}_1^+ - \dot{\vartheta}_1^-\right) + \left(\dot{s}_1^+ - \dot{s}_1^-\right) \sin \beta_1 \\ \dot{\psi}_1 = -\dot{\vartheta}_1^+ + \dot{\vartheta}_1^- \end{cases} \tag{17}$$

Kinematic equations (16) and (17) can be cast in a compact matrix form as follows:

$$\dot{\boldsymbol{U}}_G = \boldsymbol{B}_G \dot{\boldsymbol{\lambda}}, \qquad \dot{\boldsymbol{\lambda}} \geq \boldsymbol{0} \tag{18}$$

where, the 3*n* velocities ruling the rigid movements of the *n* rigid blocks have been collected in vector $\dot{\boldsymbol{U}}_G$:

$$\dot{\boldsymbol{U}}_G = \left[\dot{u}_{G_1}, \dot{v}_{G_1}, \dot{\psi}_1, \ \cdots, \dot{u}_{G_k}, \dot{v}_{G_k}, \dot{\psi}_k, \ \cdots, \dot{u}_{G_n}, \dot{v}_{G_n}, \dot{\psi}_n\right]^T \tag{19}$$

and the 4(*n* + 1) relative velocities relevant to the (*n* + 1) joints are collected in vector $\dot{\boldsymbol{\lambda}}$:

$$\dot{\boldsymbol{\lambda}} = \left[\dot{\vartheta}_1^+, \ \dot{\vartheta}_1^-, \ \dot{s}_1^+, \ \dot{s}_1^-, \ \cdots, \dot{\vartheta}_k^+, \ \dot{\vartheta}_k^-, \ \dot{s}_k^+, \ \dot{s}_k^-, \ \cdots, \dot{\vartheta}_{n+1}^+, \ \dot{\vartheta}_{n+1}^-, \ \dot{s}_{n+1}^+, \ \dot{s}_{n+1}^-\right]^T \tag{20}$$

Once centroidal compatibility matrix $\boldsymbol{B}_G$ has been initialized, its first three rows can be readily computed according to Eqs. (17):

$$\begin{aligned}
\boldsymbol{B}_G &= zeros(3n, 4n+4) \\
\boldsymbol{B}_G(1, 1{:}4) &= \left[-\left(r+\tfrac{t}{2}\right)\sin\beta_1 + y_{G_1}, +\left(r-\tfrac{t}{2}\right)\sin\beta_1 - y_{G_1}, \ \cos\beta_1, \ -\cos\beta_1\right] \\
\boldsymbol{B}_G(2, 1{:}4) &= \left[+\left(r+\tfrac{t}{2}\right)\cos\beta_1 - x_{G_1}, -\left(r-\tfrac{t}{2}\right)\cos\beta_1 + x_{G_1}, \ \sin\beta_1, \ -\sin\beta_1\right] \\
\boldsymbol{B}_G(3, 1{:}4) &= [\quad -1, \quad 1, \quad 0, \quad 0]
\end{aligned} \tag{21}$$

while the other rows can be obtained in a recursive way (*k* = 2, …, *n*), according to Eqs. (16):

$$\begin{aligned}
\boldsymbol{B}_G(3k-2, :) &= \boldsymbol{B}_G(3k-5, :) - \left(y_{G_k} - y_{G_{k-1}}\right)\boldsymbol{B}_G(3k-3, :) \\
\boldsymbol{B}_G(3k-2, \ 4k-3) &\leftarrow \boldsymbol{B}_G(3k-2, \ 4k-3) - \left(r+\tfrac{t}{2}\right)\sin\beta_k + y_{G_k} \\
\boldsymbol{B}_G(3k-2, \ 4k-2) &\leftarrow \boldsymbol{B}_G(3k-2, \ 4k-2) + \left(r-\tfrac{t}{2}\right)\sin\beta_k - y_{G_k} \\
\boldsymbol{B}_G(3k-2, \ 4k-1) &\leftarrow \boldsymbol{B}_G(3k-2, \ 4k-1) + \cos\beta_k \\
\boldsymbol{B}_G(3k-2, \ 4k) &\leftarrow \boldsymbol{B}_G(3k-2, \ 4k) - \cos\beta_k
\end{aligned} \tag{22}$$

$$\begin{aligned}
\boldsymbol{B}_G(3k-1, :) &= \boldsymbol{B}_G(3k-4, :) + \left(x_{G_k} - x_{G_{k-1}}\right)\boldsymbol{B}_G(3k-3, :) \\
\boldsymbol{B}_G(3k-1, \ 4k-3) &\leftarrow \boldsymbol{B}_G(3k-1, \ 4k-3) + \left(r+\tfrac{t}{2}\right)\cos\beta_k - x_{G_k} \\
\boldsymbol{B}_G(3k-1, \ 4k-2) &\leftarrow \boldsymbol{B}_G(3k-1, \ 4k-2) - \left(r-\tfrac{t}{2}\right)\cos\beta_k + x_{G_k} \\
\boldsymbol{B}_G(3k-1, \ 4k-1) &\leftarrow \boldsymbol{B}_G(3k-1, \ 4k-1) + \sin\beta_k \\
\boldsymbol{B}_G(3k-1, \ 4k) &\leftarrow \boldsymbol{B}_G(3k-1, \ 4k) - \sin\beta_k
\end{aligned} \tag{23}$$

$$\begin{aligned}
\boldsymbol{B}_G(3k, :) &= \boldsymbol{B}_G(3k-3, :) \\
\boldsymbol{B}_G(3k, \ 4k-3) &\leftarrow \boldsymbol{B}_G(3k, \ 4k-3) - 1 \\
\boldsymbol{B}_G(3k, \ 4k-2) &\leftarrow \boldsymbol{B}_G(3k, \ 4k-2) + 1
\end{aligned} \tag{24}$$

Finally, the kinematic constraints acting on the left side of the arch (joint *n* + 1, of local inclination β_{n+1}) yield the following three kinematic equations, directly obtained from Eqs. (16)

by assuming $k = n + 1$, i.e. by considering the basement on the left as the $(n + 1)$–*th* block and setting to zero the velocities related to it:

$$\begin{cases} 0 = -\left[\left(r+\frac{t}{2}\right)\dot{\vartheta}_{n+1}^{+} - \left(r-\frac{t}{2}\right)\dot{\vartheta}_{n+1}^{-}\right]\sin\beta_{n+1} + \\ \qquad\qquad +(\dot{s}_{n+1}^{+} - \dot{s}_{n+1}^{-})\cos\beta_{n+1} + \dot{u}_{G_n} + y_{G_n}\dot{\psi}_n \\ 0 = +\left[\left(r+\frac{t}{2}\right)\dot{\vartheta}_{n+1}^{+} - \left(r-\frac{t}{2}\right)\dot{\vartheta}_{n+1}^{-}\right]\cos\beta_{n+1} + \\ \qquad\qquad +(\dot{s}_{n+1}^{+} - \dot{s}_{n+1}^{-})\sin\beta_{n+1} + \dot{v}_{G_n} - x_{G_n}\dot{\psi}_n \\ 0 = \dot{\psi}_n - \dot{\vartheta}_{n+1}^{+} + \dot{\vartheta}_{n+1}^{-} \end{cases} \tag{25}$$

These equations represent three constraints on the whole set of kinematic variable rates $\dot{\boldsymbol{\lambda}}$:

$$\boldsymbol{B}\dot{\boldsymbol{\lambda}} = \boldsymbol{0}, \qquad \dot{\boldsymbol{\lambda}} \geq \boldsymbol{0} \tag{26}$$

where, the velocities relevant to the *n*–th block (i.e. $\dot{u}_{G_n}, \dot{v}_{G_n}, \dot{\psi}_n$) can be obtained from the last three rows of matrix $\boldsymbol{B}_G$. Then, global compatibility matrix $\boldsymbol{B}$, whose size is $3 \times (4n + 4)$, can still be built in a recursive way as follows:

$$\begin{aligned} \boldsymbol{B}(1,:) &= \boldsymbol{B}_G(3n-2,:) + y_{G_n}\,\boldsymbol{B}_G(3n,:) \\ \boldsymbol{B}(1,\ 4n+1) &\leftarrow \boldsymbol{B}(1,\ 4n+1) - \left(r+\frac{t}{2}\right)\sin\beta_{n+1} \\ \boldsymbol{B}(1,\ 4n+2) &\leftarrow \boldsymbol{B}(1,\ 4n+2) + \left(r-\frac{t}{2}\right)\sin\beta_{n+1} \\ \boldsymbol{B}(1,\ 4n+3) &\leftarrow \boldsymbol{B}(1,\ 4n+3) + \cos\beta_{n+1} \\ \boldsymbol{B}(1,\ 4n+4) &\leftarrow \boldsymbol{B}(1,\ 4n+4) - \cos\beta_{n+1} \end{aligned} \tag{27}$$

$$\begin{aligned} \boldsymbol{B}(2,:) &= \boldsymbol{B}_G(3n-1,:) - x_{G_n}\,\boldsymbol{B}_G(3n,:) \\ \boldsymbol{B}(2,\ 4n+1) &\leftarrow \boldsymbol{B}(2,\ 4n+1) + \left(r+\frac{t}{2}\right)\cos\beta_{n+1} \\ \boldsymbol{B}(2,\ 4n+2) &\leftarrow \boldsymbol{B}(2,\ 4n+2) - \left(r-\frac{t}{2}\right)\cos\beta_{n+1} \\ \boldsymbol{B}(2,\ 4n+3) &\leftarrow \boldsymbol{B}(2,\ 4n+3) + \sin\beta_{n+1} \\ \boldsymbol{B}(2,\ 4n+4) &\leftarrow \boldsymbol{B}(2,\ 4n+4) - \sin\beta_{n+1} \end{aligned} \tag{28}$$

$$\begin{aligned} \boldsymbol{B}(3,:) &= \boldsymbol{B}_G(3n,:) \\ \boldsymbol{B}(3,\ 4n+1) &\leftarrow \boldsymbol{B}(3,\ 4n+1) - 1 \\ \boldsymbol{B}(3,\ 4n+2) &\leftarrow \boldsymbol{B}(3,\ 4n+2) + 1 \end{aligned} \tag{29}$$

The whole kinematics of the arch, within the hypothesis of non–compenetrating blocks (Figure 2), can be described by a set of relative velocities $\dot{\boldsymbol{\lambda}}$ fulfilling compatibility relations (26). Within this set, a generic collapse mechanism of the masonry arch can be

considered as an "*admissible mechanism*" when the external power produced by the load (e.g. the self–weight of the arch) is non–negative:

$$\dot{L}_e = \boldsymbol{w}^T \dot{\boldsymbol{U}}_G \geq 0, \qquad \boldsymbol{w} = \begin{bmatrix} \boldsymbol{w}_1 \\ \vdots \\ \boldsymbol{w}_k \\ \vdots \\ \boldsymbol{w}_n \end{bmatrix}, \qquad \boldsymbol{w}_k = \begin{bmatrix} 0 \\ -(\beta_{k+1} - \beta_k)\, \gamma t d\, r \\ 0 \end{bmatrix} \tag{30}$$

where $\boldsymbol{w}$ is the weight array of the masonry blocks separated by the various radial joints (note that $\boldsymbol{w}$ components are assumed to be positive upward).

Finally, the velocity field can be arbitrarily normalized by setting:

$$\boldsymbol{p}^T \dot{\boldsymbol{\lambda}} = 1, \qquad p(k) = 1, \qquad k = 1, \dots, n+1 \tag{31}$$

Summarizing the above conditions, an *"admissible kinematic configuration"* is characterized by a set of relative velocities $\dot{\boldsymbol{\lambda}}$ fulfilling the following relationships:

$$\boldsymbol{B}\dot{\boldsymbol{\lambda}} = \boldsymbol{0}, \quad \dot{\boldsymbol{s}}^{+T} \dot{\boldsymbol{s}}^{-} = \dot{\boldsymbol{\lambda}}^T \boldsymbol{B}_s^{+T} \boldsymbol{B}_s^{-} \dot{\boldsymbol{\lambda}} = 0, \quad \dot{\boldsymbol{\lambda}} \geq \boldsymbol{0}, \quad \dot{L}_e = \boldsymbol{w}^T \boldsymbol{B}_G \dot{\boldsymbol{\lambda}} \geq 0, \quad \boldsymbol{p}^T \dot{\boldsymbol{\lambda}} = 1 \tag{32}$$

in which Boolean matrices $\boldsymbol{B}_s^+$ and $\boldsymbol{B}_s^-$ are used to extract, respectively, sliding kinematic variables $\dot{\boldsymbol{s}}^+$ and $\dot{\boldsymbol{s}}^-$ from kinematic variable vector $\dot{\boldsymbol{\lambda}}$:

$$\dot{\boldsymbol{s}}^+ = \boldsymbol{B}_s^+ \dot{\boldsymbol{\lambda}}, \qquad \dot{\boldsymbol{s}}^- = \boldsymbol{B}_s^- \dot{\boldsymbol{\lambda}} \tag{33}$$

2.3 Static description

The three cross–section internal actions representing the state of macroscopic stress within the generic masonry arch joint are: compression axial force (N), shear force (T) and bending moment (M); reactions H, V and W, at the arch basement on the right ($\beta = \beta_1$) are taken as redundant reactions, as shown in Figure 7.

The internal actions can readily be computed by the equilibrium of the generic part of the arch, according to Heyman uniform self–weight distribution along geometrical centerline, as (see Figure 7):

$$\begin{cases} N(\beta) = H\sin\beta + V\cos\beta - \gamma t d\, r\, (\beta - \beta_1)\cos\beta \\ T(\beta) = H\cos\beta - V\sin\beta + \gamma t d\, r\, (\beta - \beta_1)\sin\beta \\ M(\beta) = -H\, r\, (\sin\beta - \sin\beta_1) + V\, r\, (\cos\beta_1 - \cos\beta) + W + \\ \qquad\qquad + \gamma t d\, r^2 \left((\beta - \beta_1)\cos\beta - (\sin\beta - \sin\beta_1)\right) \end{cases} \tag{34}$$

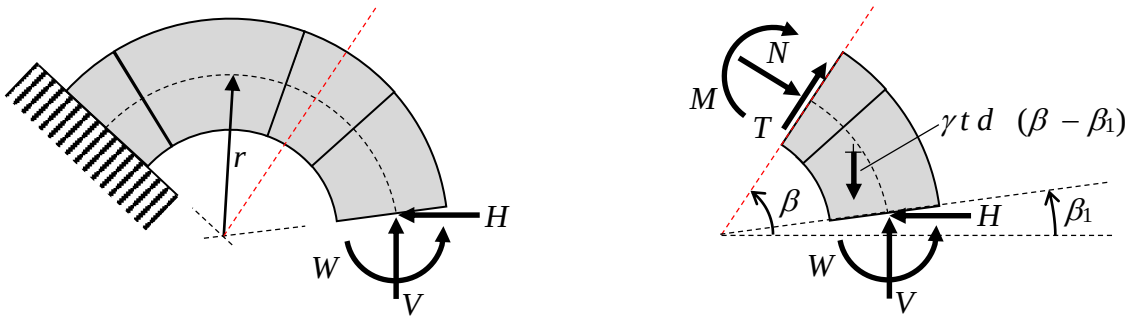

Figure 7: Sketch with redundant reactions and internal actions within the circular masonry arch. Figure also reports the block weight, which applies as well in the writing of equilibrium Eqs. (34).

At the k–th joint, two sets of conditions are enforced. The resulting normal force has to act within the arch thickness, namely the (centroidal) axial force ($N_k = N(\beta_k)$) and the bending moment ($M_k = M(\beta_k)$) must fulfill the following inequalities:

$$-N_k \frac{t}{2} \le M_k \le N_k \frac{t}{2}, \qquad k = 1, \dots, n+1 \tag{35}$$

Contemporarily, the axial (N_k) and shear ($T_k = T(\beta_k)$) forces must comply with Coulomb's friction relationship:

$$-\mu\, N_k \le T_k \le \mu\, N_k, \qquad k = 1, \dots, n+1 \tag{36}$$

The above $4(n+1)$ inequalities can be cast according to the sequence adopted for the (work–conjugate) kinematic variables collected in the $\dot{\boldsymbol{\lambda}}$ vector, Eq. (20):

$$\boldsymbol{\varphi} = \begin{bmatrix} \boldsymbol{\varphi}_1 \\ \cdots \\ \boldsymbol{\varphi}_k \\ \cdots \\ \boldsymbol{\varphi}_{n+1} \end{bmatrix} \leq \mathbf{0}, \qquad \boldsymbol{\varphi}_k = \begin{bmatrix} M_k - N_k \frac{t}{2} \\ -M_k - N_k \frac{t}{2} \\ T_k - \mu\, N_k \\ -T_k - \mu\, N_k \end{bmatrix} \tag{37}$$

Relationships (34) and (37) define an *"admissible static configuration"* within the arch, the independent variables being three redundant reactions *H*, *V* and *W*:

$$\boldsymbol{\varphi} = \boldsymbol{A}\,\boldsymbol{H} + \boldsymbol{T}^w \leq \mathbf{0}, \quad \boldsymbol{A} = \begin{bmatrix} \boldsymbol{\varphi}_1^H, & \boldsymbol{\varphi}_1^V, & \boldsymbol{\varphi}_1^W \\ \cdots, & \cdots, & \cdots \\ \boldsymbol{\varphi}_k^H, & \boldsymbol{\varphi}_k^V, & \boldsymbol{\varphi}_k^W \\ \cdots, & \cdots, & \cdots \\ \boldsymbol{\varphi}_{n+1}^H, & \boldsymbol{\varphi}_{n+1}^V, & \boldsymbol{\varphi}_{n+1}^W \end{bmatrix}, \quad \boldsymbol{H} = \begin{bmatrix} H \\ V \\ W \end{bmatrix}, \quad \boldsymbol{T}^w = \begin{bmatrix} \boldsymbol{T}_1^w \\ \vdots \\ \boldsymbol{T}_k^w \\ \vdots \\ \boldsymbol{T}_{n+1}^w \end{bmatrix} \tag{38}$$

where:

$$\boldsymbol{\varphi}_k^H = \begin{bmatrix} -\left(r + \frac{t}{2}\right) \sin\beta_k + r \sin\beta_1 \\ \left(r - \frac{t}{2}\right) \sin\beta_k - r \sin\beta_1 \\ \cos\beta_k - \mu \sin\beta_k \\ -\cos\beta_k - \mu \sin\beta_k \end{bmatrix}, \quad \boldsymbol{\varphi}_k^V = \begin{bmatrix} -\left(r + \frac{t}{2}\right) \cos\beta_k + r \cos\beta_1 \\ \left(r - \frac{t}{2}\right) \cos\beta_k - r \cos\beta_1 \\ -\sin\beta_k - \mu \cos\beta_k \\ \sin\beta_k - \mu \cos\beta_k \end{bmatrix} \tag{39}$$

$$\boldsymbol{\varphi}_k^W = \begin{bmatrix} 1 \\ -1 \\ 0 \\ 0 \end{bmatrix}, \quad \boldsymbol{T}_k^w = \gamma t d\, r \begin{bmatrix} \left(r + \frac{t}{2}\right)(\beta_k - \beta_1)\cos\beta_k - r\,(\sin\beta_k - \sin\beta_1) \\ -\left(r - \frac{t}{2}\right)(\beta_k - \beta_1)\cos\beta_k + r\,(\sin\beta_k - \sin\beta_1) \\ (\beta_k - \beta_1)(\sin\beta_k + \mu\cos\beta_k) \\ (\beta_k - \beta_1)(-\sin\beta_k + \mu\cos\beta_k) \end{bmatrix} \tag{40}$$

2.4 Complementarity conditions

Previous relations (32) and (38) define the sets of *"admissible kinematics"* and *"admissible statics"*, respectively. It is worth noting that a limit equilibrium configuration at incipient collapse requires the fulfillment of both of such sets of admissibility relations and of the "orthogonality" condition among them, namely:

$$\begin{cases} \dot{\vartheta}_k^+\ \varphi_k(1) = \dot{\vartheta}_k^+ \left(M_k - N_k \frac{t}{2}\right) = 0 \\ \dot{\vartheta}_k^-\ \varphi_k(2) = \dot{\vartheta}_k^- \left(-M_k - N_k \frac{t}{2}\right) = 0 \\ \dot{s}_k^+\ \varphi_k(3) = \dot{s}_k^+\ (T_k - \mu\, N_k) = 0 \\ \dot{s}_k^-\ \varphi_k(4) = \dot{s}_k^-\ (-T_k - \mu\, N_k) = 0 \end{cases}, \qquad k = 1, \ldots, n+1 \tag{41}$$

In general terms, in a limit equilibrium configuration at incipient collapse, kinematics ($\dot{\boldsymbol{\lambda}}$) and static (**H**) variables shall fulfill the following *complementarity problem* (see e.g. [59]):

$$\begin{cases} f = -\boldsymbol{\varphi}^T \dot{\boldsymbol{\lambda}} = 0 \\ \boldsymbol{\varphi} = \boldsymbol{A}\,\boldsymbol{H} + \boldsymbol{T}^w \leq \mathbf{0} \\ \boldsymbol{B}\dot{\boldsymbol{\lambda}} = \mathbf{0} \\ \dot{L}_e = \boldsymbol{w}^T \mathbf{B}_G \dot{\boldsymbol{\lambda}} \geq 0 \\ \boldsymbol{p}^T \dot{\boldsymbol{\lambda}} = 1 \\ \dot{\boldsymbol{\lambda}} \geq \mathbf{0} \\ \dot{\boldsymbol{s}}^{+T} \dot{\boldsymbol{s}}^- = \dot{\boldsymbol{\lambda}}^T \boldsymbol{B}_S^{+T} \boldsymbol{B}_S^- \dot{\boldsymbol{\lambda}} = 0 \end{cases} \tag{42}$$

Additionally, a convenient solution to non–linear complementarity system (42) may be obtained by the following *non–linear programming problem*, in which the (nonlinear) orthogonality condition on variables $\boldsymbol{\varphi}$ and $\dot{\boldsymbol{\lambda}}$ is used as objective function (see e.g. [60]):

$$f_{min} = \min_{\dot{\boldsymbol{\lambda}},\, \boldsymbol{H}} \left\{ -\boldsymbol{\varphi}^T \dot{\boldsymbol{\lambda}} \;\middle|\; \begin{array}{c} \boldsymbol{\varphi} = \boldsymbol{A}\,\boldsymbol{H} + \boldsymbol{T}^w \leq \mathbf{0} \\ \boldsymbol{B}\dot{\boldsymbol{\lambda}} = \mathbf{0} \\ \dot{L}_e = \boldsymbol{w}^T \mathbf{B}_G \dot{\boldsymbol{\lambda}} \geq 0 \\ \boldsymbol{p}^T \dot{\boldsymbol{\lambda}} = 1 \\ \dot{\boldsymbol{\lambda}} \geq \mathbf{0} \\ \dot{\boldsymbol{s}}^{+T} \dot{\boldsymbol{s}}^- = \dot{\boldsymbol{\lambda}}^T \boldsymbol{B}_S^{+T} \boldsymbol{B}_S^- \dot{\boldsymbol{\lambda}} = 0 \end{array} \right\} \tag{43}$$

when, in addition, it results that

$$f_{min} = 0 \tag{44}$$

Further, also the orthogonality condition on variables $\dot{\boldsymbol{s}}^+$ and $\dot{\boldsymbol{s}}^-$ may be conveniently transferred to the objective function by adding (non–negative) scalar product $\dot{\boldsymbol{s}}^{+T} \dot{\boldsymbol{s}}^-$ to (non–negative) term $-\boldsymbol{\varphi}^T \dot{\boldsymbol{\lambda}}$. In this way, the *non–linear programming problem* turns out to be characterized only by linear constraints:

$$f_{min} = \min_{\dot{\boldsymbol{\lambda}},\, \boldsymbol{H}} \left\{ -\boldsymbol{\varphi}^T \dot{\boldsymbol{\lambda}} + \dot{\boldsymbol{s}}^{+T} \dot{\boldsymbol{s}}^- \;\middle|\; \begin{array}{c} \boldsymbol{\varphi} = \boldsymbol{A}\,\boldsymbol{H} + \boldsymbol{T}^w \leq \mathbf{0} \\ \boldsymbol{B}\dot{\boldsymbol{\lambda}} = \mathbf{0} \\ \dot{L}_e = \boldsymbol{w}^T \mathbf{B}_G \dot{\boldsymbol{\lambda}} \geq 0 \\ \boldsymbol{p}^T \dot{\boldsymbol{\lambda}} = 1 \\ \dot{\boldsymbol{\lambda}} \geq \mathbf{0} \\ \dot{\boldsymbol{s}}^+ = \boldsymbol{B}_S^+ \dot{\boldsymbol{\lambda}}, \quad \dot{\boldsymbol{s}}^- = \boldsymbol{B}_S^- \dot{\boldsymbol{\lambda}} \end{array} \right\} \tag{45}$$

where, the solution to original problem (42) is obtained only if condition (44) is again satisfied.

Notice that in programming problems (43) or (45) thickness *t* and friction coefficient μ are assumed as free parameters to be arbitrarily changed, to get to a zero value as an optimum value for objective function *f*, as stated in Eq. (44).

Finally, it is worth underlining that multiple solutions to (non−convex) problem (42), and thus to programming problems (43) or (45), with condition (44), may generally be expected (see e.g. [61] and [70−73]).

2.5 Remarks on possible outcoming results

From an engineering point of view, the main goal of the present investigation is searching for the minimum masonry arch thickness for which "safe conditions can be guaranteed", at reducing friction. This quest assumes a clear meaning both in classical Limit Analysis (LA), according to the Lower−Bound ("static") theorem, and in its consolidated extensions to arch analysis (see e.g. [1−4,17]). However, the issue of non−normality of the flow rule linked to the presence of possible sliding failure, as here related to a reducing friction, may come to spoil the picture because in that case the "uniqueness" (or "mixed") theorem of LA shall not provide, in general, a unique solution in terms of load multiplier (thus, here, in terms of arch thickness). Despite that, for some class of arch problems, including symmetric arches, as claimed by Casapulla and Lauro [35] and cited by Gilbert et al. [36], the present formulation is totally general and should be able to locate if non−uniqueness in arch thickness in the least critical condition may arise or not. Toward that, the present work attempts to address the issue by a novel numerical implementation relying on the solution of complementarity problem (42) or of non−linear programming problem (43) or (45).

In that concern, the activation of the Coulombian frictional behaviour violates one of the main hypotheses of LA, i.e. the *normality of the flow rule*. In this framework, in the examples discussed in the following, for given thickness t and friction coefficient μ, a (strict) "safe condition" is assumed to hold when there exists a set of redundant reactions $\mathbf{H}$ for which consistency conditions (38) are fulfilled (i.e. an admissible statics can be found), but it is not possible to find any compatible kinematics (32) (i.e. an admissible mechanism) complying with "orthogonality" relations (41).

A "safe condition" is also assumed when an optimum solution can be given to non−linear programming problems (43) or (45), but $\boldsymbol{\varphi}^T\dot{\boldsymbol{\lambda}} < 0$ results for it; this means that both an admissible statics and an admissible mechanism can be found, but they do not comply with "orthogonality" relations (41), namely they cannot represent a limiting condition.

Differently from above, the classical "limit equilibrium condition" is characterized by the existence of an admissible statics (Eqs. (38)) and an admissible kinematics (Eqs. (32)), both fulfilling "orthogonality" relations (41). This means that the optimum solution to problems (43) or (45) yields $\boldsymbol{\varphi}^T\dot{\boldsymbol{\lambda}} = 0$.

Finally, in the following numerical examples, the unfeasibility of problems (43) or (45) is generally due to the violation of consistency conditions (38), i.e. when it is not possible to find an admissible statics for the given geometry and friction coefficient. In this case, the arch collapse is eventually of a dynamic kind.

Further considerations on the outcoming results are supplied in next Section 3 (see Figures 24–29 and relevant remarks).

3 NUMERICAL RESULTS

Main numerical results, obtained by non−linear programming procedures (43) or (45) out of a comprehensive numerical investigation on the self−standing conditions of symmetric circular masonry arches at reducing friction, are gathered in the present section, as resumed by the following selected pictures (Figures 8–30). Specifically, overall arch openings are considered,

for both undercomplete and overcomplete (horseshoe) arches, with comparison as well to the classical reference case of the complete semicircular arch, considering the various ranges of the friction coefficient, leading to changes in the arising collapse mode of the masonry arch, and relevant least thickness condition.

The represented figures depict both the collapse mechanism of the arch (notice that, here, symmetry is not pre–imposed) and the eccentricity lines of ratio M/N (*line of thrust*, i.e. locus of pressure points) and ratio T/N (that may be named *line of friction*[1], defined as $T/N/\mu \cdot t/2$) within the arch. The simultaneous visualization of the line of friction concept shall originally help here in the investigation of the effects of arising limited friction.

Non–linear programming procedures (43) or (45) have been implemented, after an appropriate normalization of variables, and run within MATLAB®; (built–in) optimization function "*fmincon*" and either the *"interior point"* or the "*active set*" minimization algorithm have been used, with tolerances kept at 10^{-10}.

Some of the results shown in following Figures 8–30 turn out to be fully coherent with earlier ones independently derived in [18], showing the natural mutual consistency of the adopted approaches. The reported results constitute a selection and representative sampling of the outcomes that can be achieved by the present numerical methodology, and record all the competent collapse mechanisms that can be traced at variable (reducing) friction coefficient and arch thickness, for different opening angles of the circular masonry arch with radial joints.

Figures 8–23 report, for each of them: on top the characteristic data of the case (being $\alpha_s = -\beta_1$, the angular location of the shoulder joint, according to the right sketch in Figure 7); in the centre, the plot of the eccentricities of the line of thrust and of the line of friction within the arch (once such lines touch the extremes of the arch, at the intrados and/or at the extrados, a rotational hinge joint at angular position β_N, or a sliding joint at angular position β_T, appear, respectively); at the bottom, the recorded collapse mechanism, belonging to the following species (for the specification of the collapse mechanism, refer to the caption at the bottom of each figure):

- purely rotational (classical Heymanian one);
- mixed sliding–rotational (with rotation at the crown);
- mixed rotational–sliding (with rotation at the shoulders);
- mixed rotational–sliding (with both rotation and sliding at the shoulders);
- purely sliding;
- overturning collapse (with a two–block separation at the crown).

Five sample values of the angle of embrace of the arch (as measured with reference to the classical conformation of the complete semicircular arch, $\alpha_s = 0$; for both undercomplete, $\alpha_s < 0$ and overcomplete (horseshoe) arches, $\alpha_s > 0$) are adopted (as resumed in Table 1), to show and highlight all the structural features that can be scrutinized out of the present numerical analysis (presentation is organized per angle of embrace of the arch, see again resuming Table 1). The increase in arch thickness in the critical condition becomes rather visible, with the type of collapse that is clearly ruled by the amount of underlying friction. The position of the inner failure joint, either rotational or sliding, varies, as it was expected from first earlier results reported in [18,20].

[1] This term is liberally introduced here; the authors are not aware of possible previous uses in the literature.

α_s [rad]	α_s [deg]	Figures
$-\pi/6$	−30	8–10
0	0	11–13
$\pi/6$	30	14–16
1	57.3	17–19
1.15	65.9	20–23

Table 1: Resuming frame of selected and reported cases, and relevant figures in the attached presentation.

$$\alpha_s = -\frac{\pi}{6}; \qquad \beta_N = 0.88207486, \qquad \eta = 0.022848202, \qquad \mu \geq 0.14472273$$

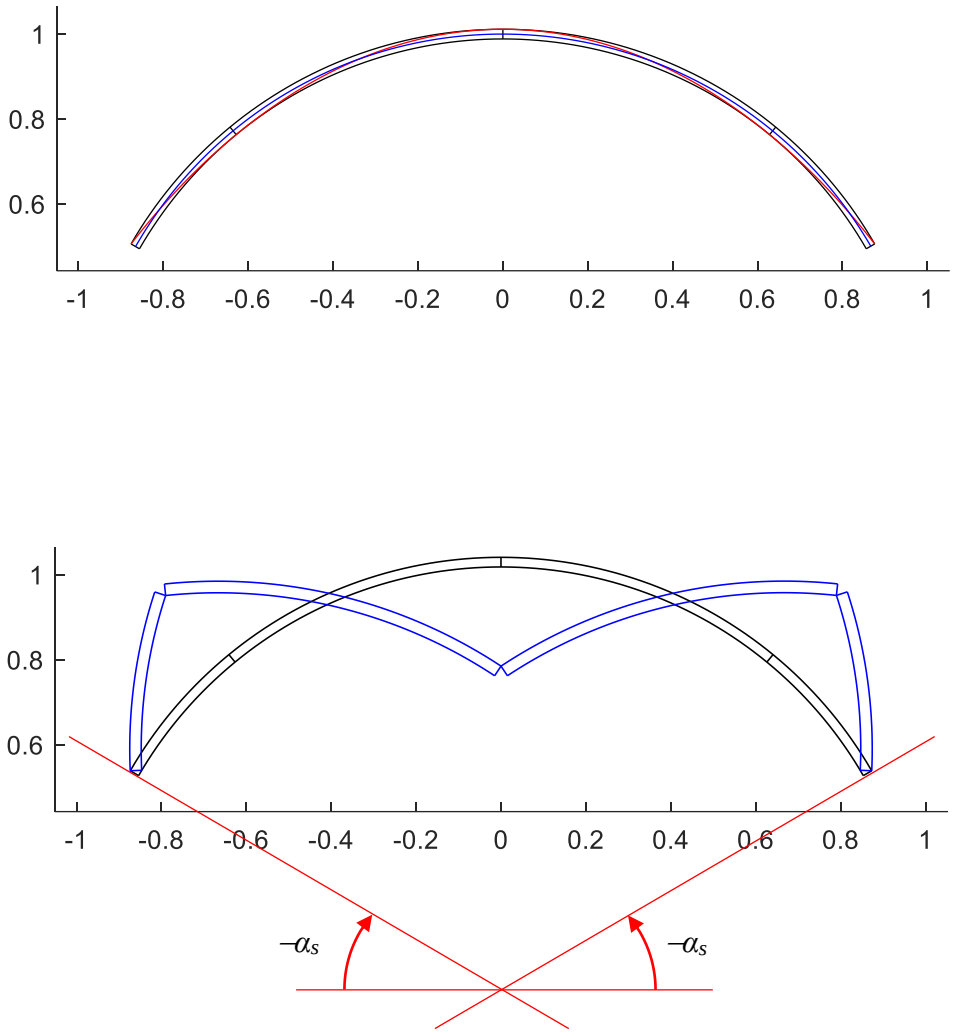

Figure 8: Characteristic values (top); lines of eccentricity (centre); collapse mechanism (bottom): purely rotational collapse.

$$\alpha_s = -\frac{\pi}{6}; \quad 0.094375852 \leq \mu \leq 0.14472273, \quad 0.049002368 \geq \eta \geq 0.022848202$$

$$0.75740905 \leq \beta_N \leq 0.88207486$$

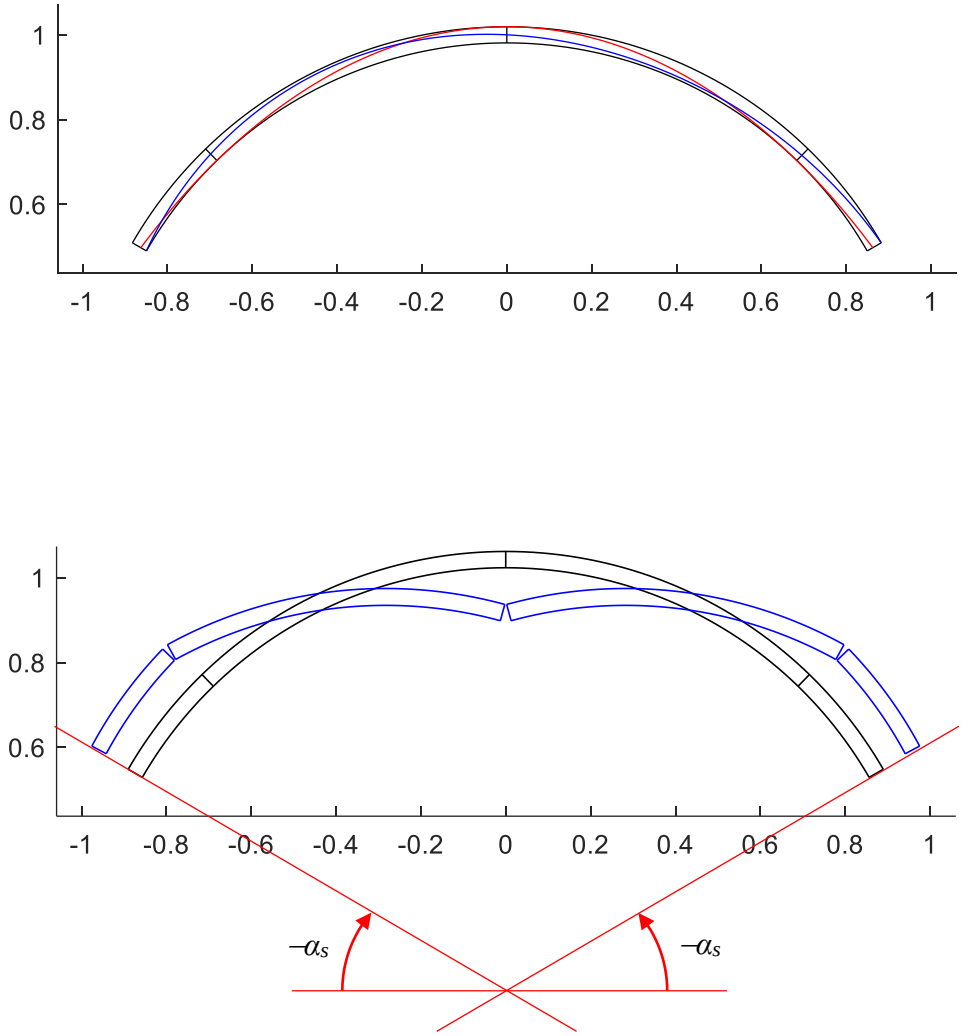

Figure 9: Characteristic values (top); lines of eccentricity (centre); collapse mechanism (bottom): mixed sliding–rotational collapse.

$$\alpha_s = -\frac{\pi}{6}, \qquad \mu = 0.094375852, \qquad \eta \geq 0.049002368, \qquad \beta_T = 1.13435616$$

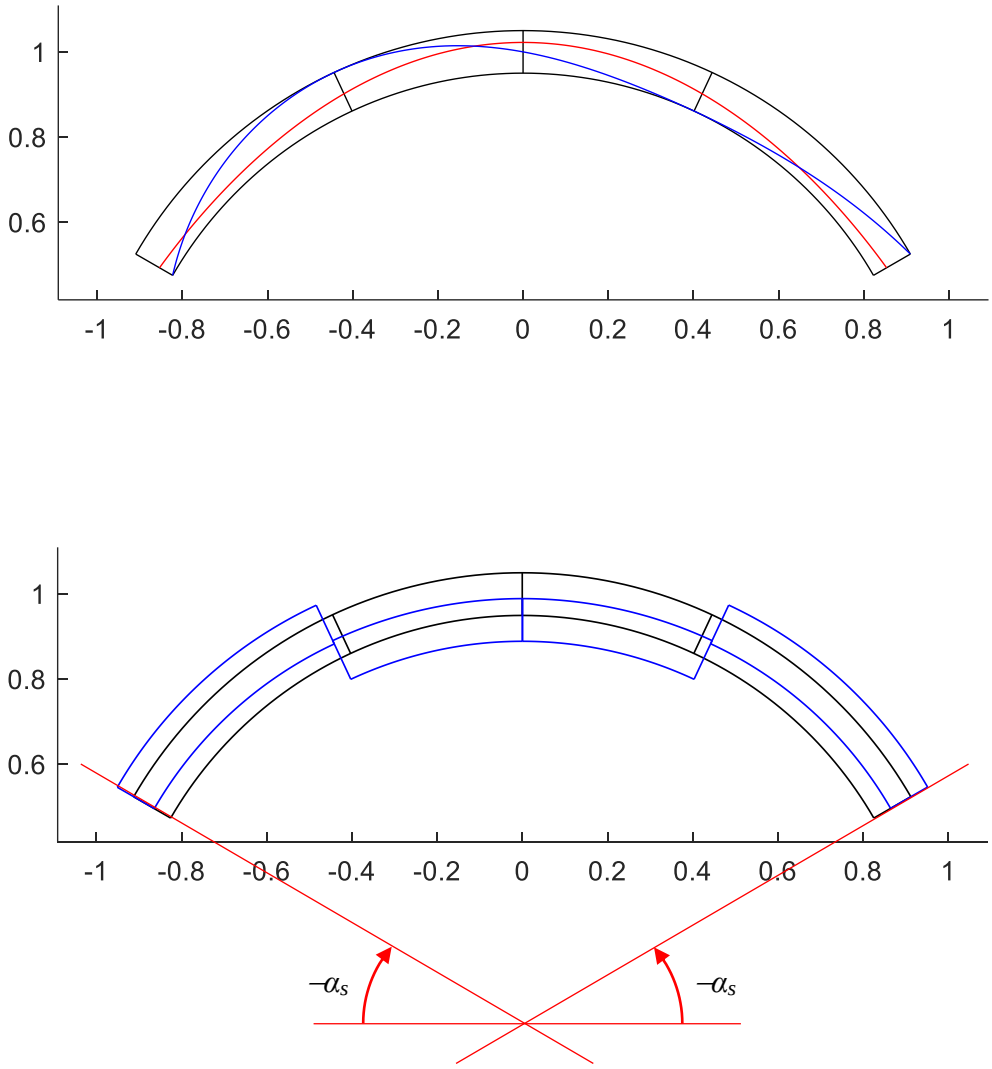

Figure 10: Characteristic values (top); lines of eccentricity (centre); collapse mechanism (bottom): purely sliding collapse.

$$\alpha_s = 0, \qquad \mu \geq 0.39583204, \qquad \eta = 0.10742645, \qquad \beta_N = 0.61965572$$

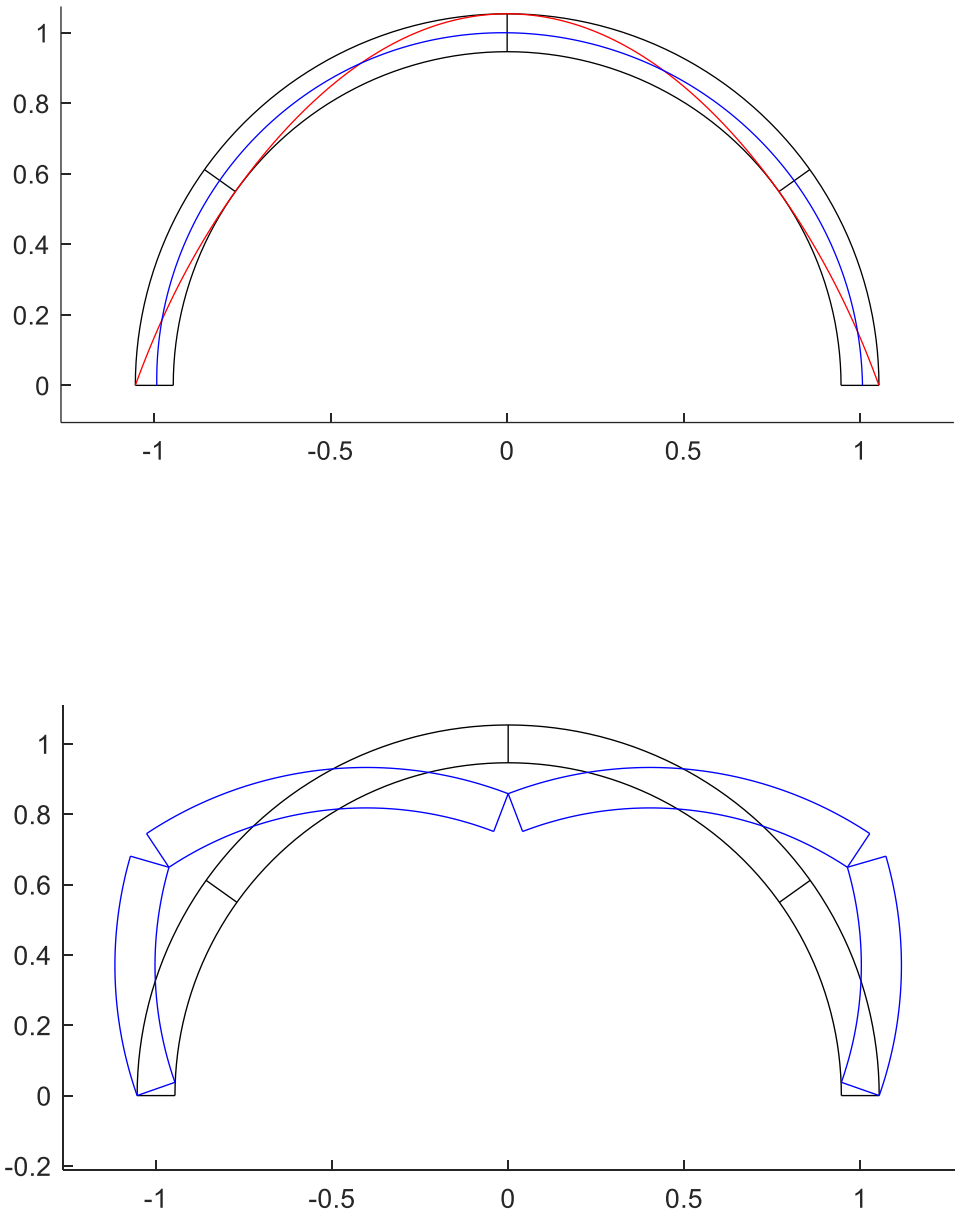

Figure 11: Characteristic values (top); lines of eccentricity (centre); collapse mechanism (bottom): purely rotational collapse.

$$\alpha_s = 0, \quad 0.30921544 \leq \mu \leq 0.39583204, \quad 0.20063732 \geq \eta \geq 0.10742645$$
$$0.51463788 \leq \beta_N \leq 0.61965572$$

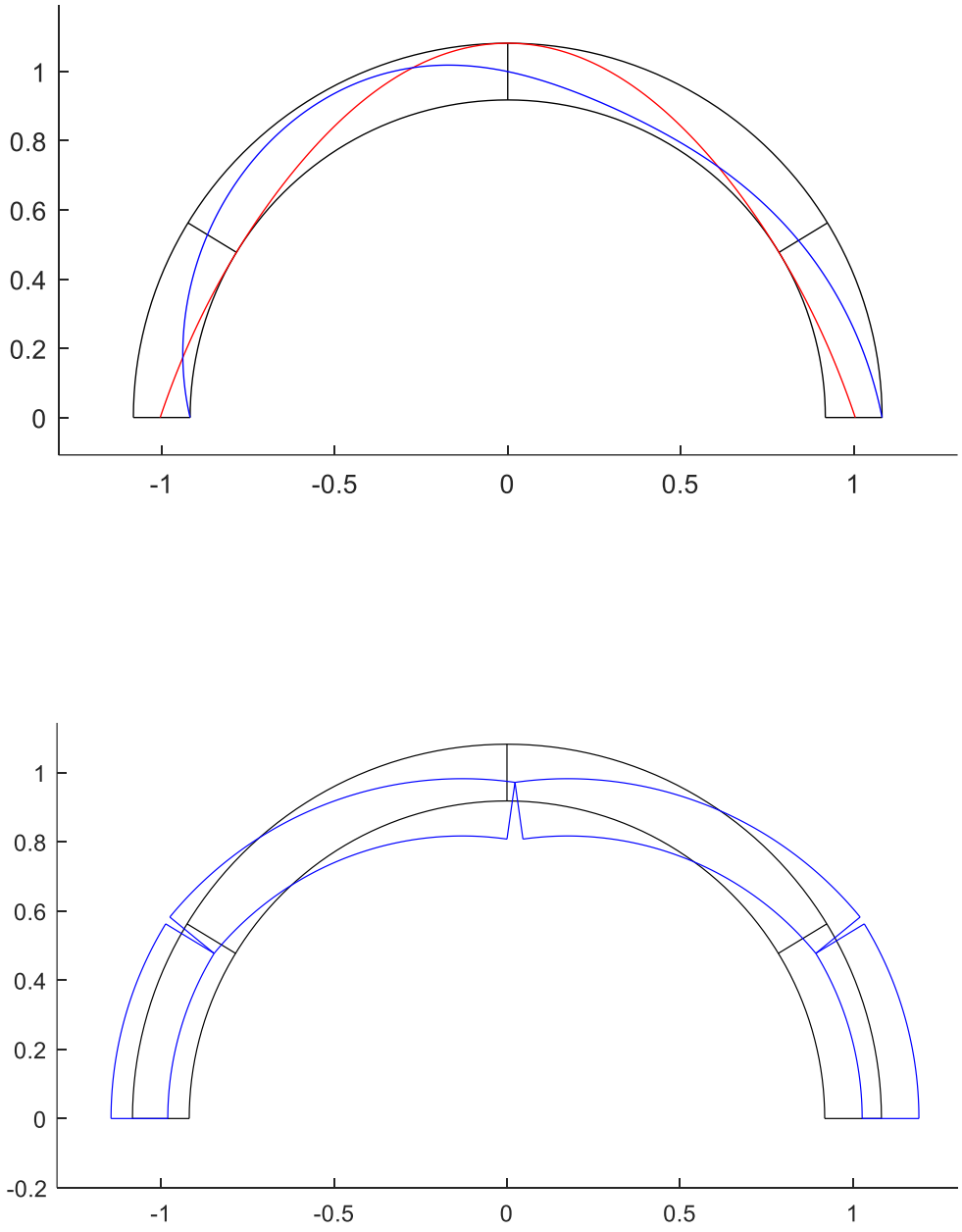

Figure 12: Characteristic values (top); lines of eccentricity (centre); collapse mechanism (bottom): mixed sliding–rotational collapse.

$$\alpha_s = 0, \quad \mu = 0.30921544, \quad \eta \geq 0.20063732, \quad \beta_T = 1.07100044$$

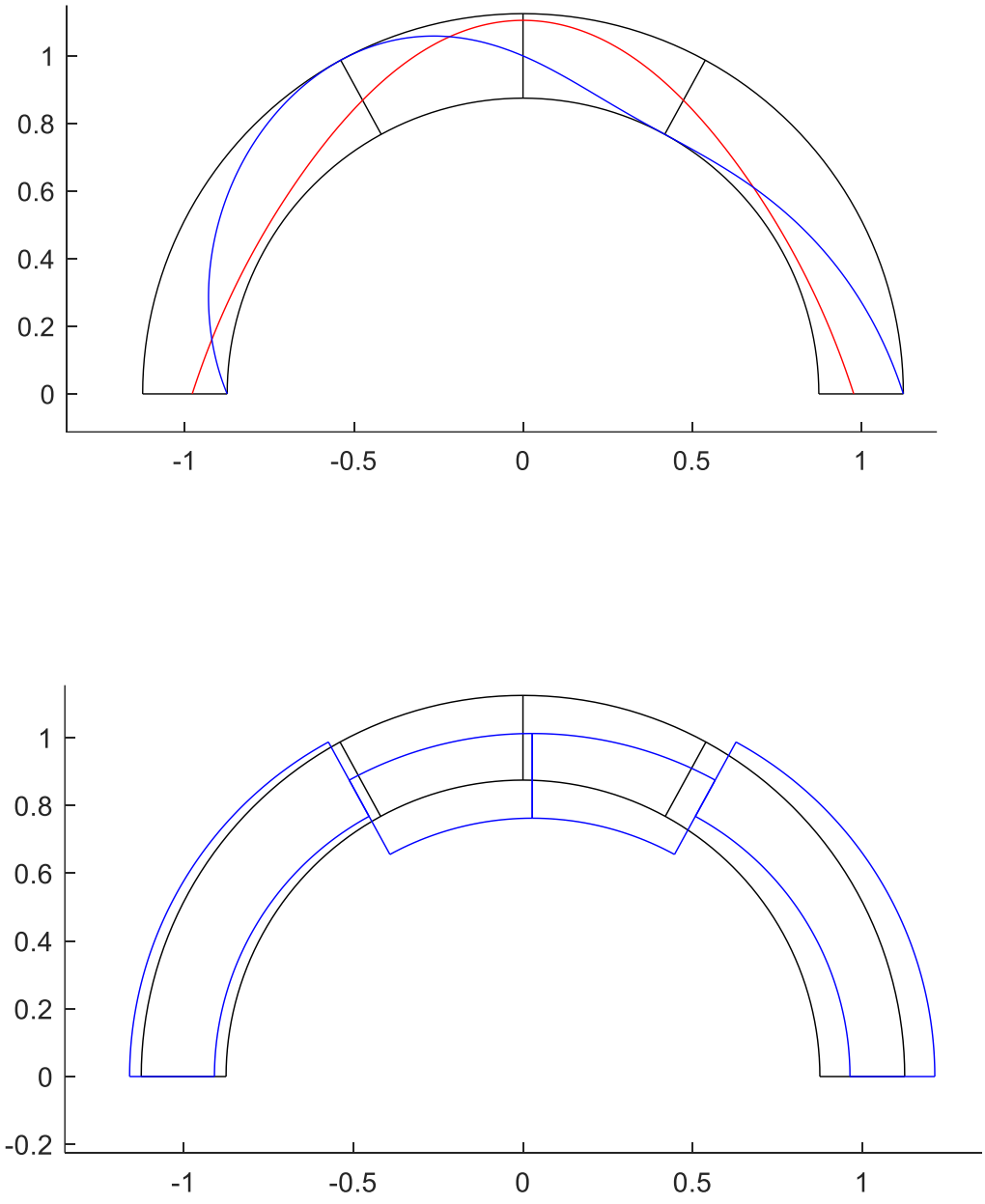

Figure 13: Characteristic values (top); lines of eccentricity (centre); collapse mechanism (bottom): purely sliding collapse.

$$\alpha_s = +\frac{\pi}{6}, \quad \beta_N = 0.45365963, \quad \eta = 0.32654664, \quad \mu \geq 0.82361489$$

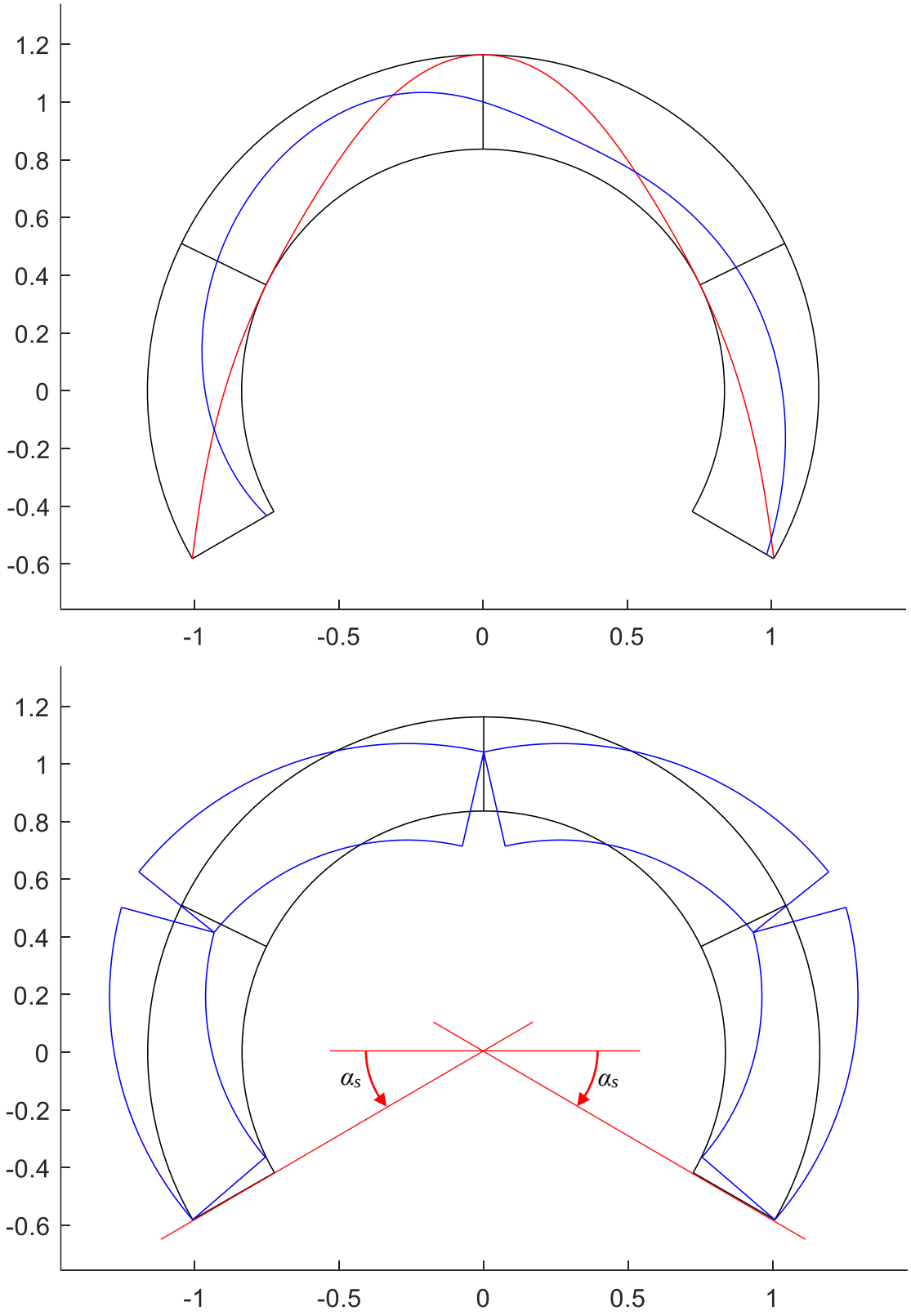

Figure 14: Characteristic values (top); lines of eccentricity (centre); collapse mechanism (bottom): purely rotational collapse.

$$\alpha_s = +\frac{\pi}{6}, \qquad 0.73904014 \leq \mu \leq 0.82361489, \qquad 0.45943411 \geq \eta \geq 0.32654664$$

$$0.44355547 \leq \beta_N \leq 0.45365963$$

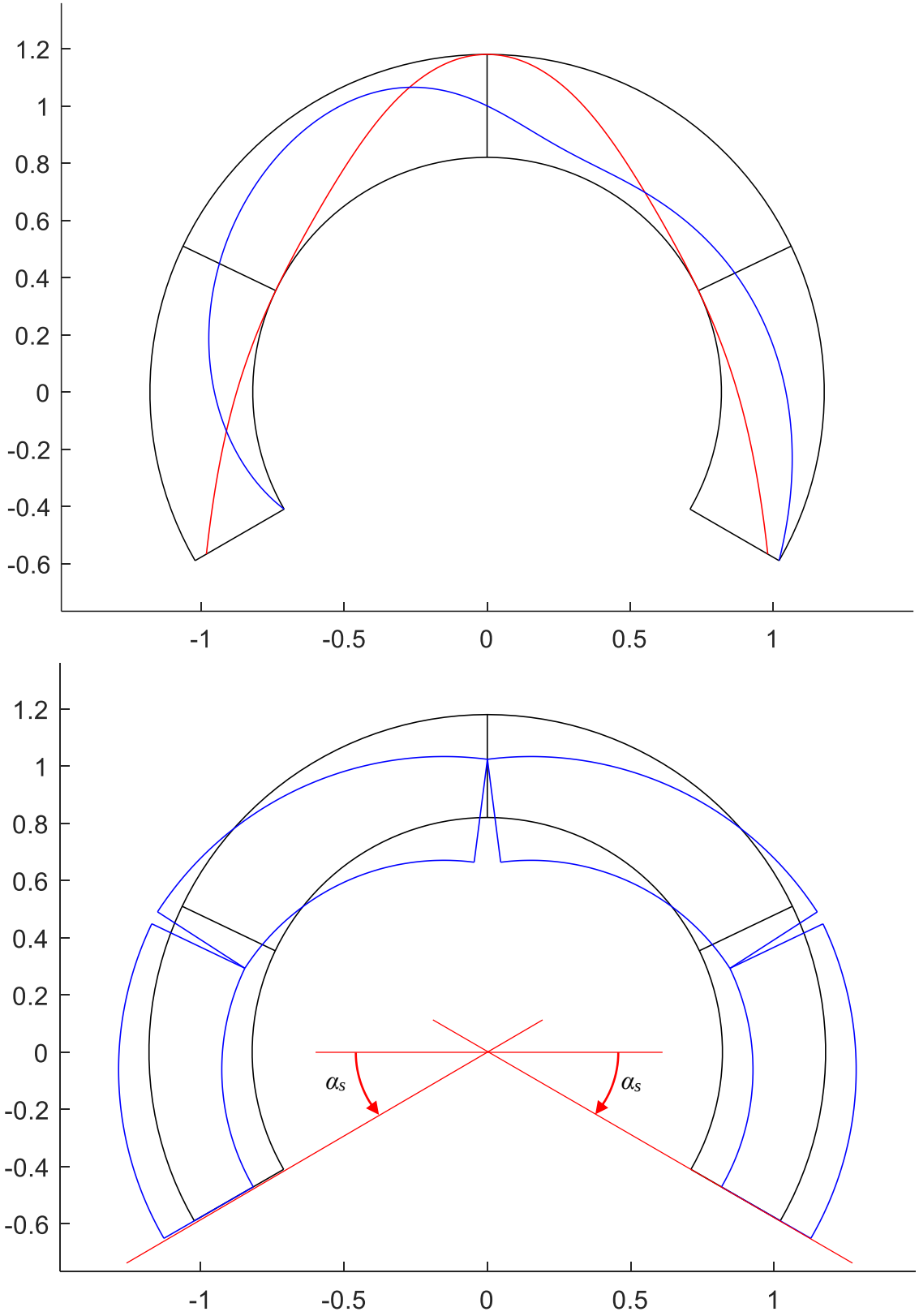

Figure 15: Characteristic values (top); lines of eccentricity (centre); collapse mechanism (bottom): mixed sliding–rotational collapse.

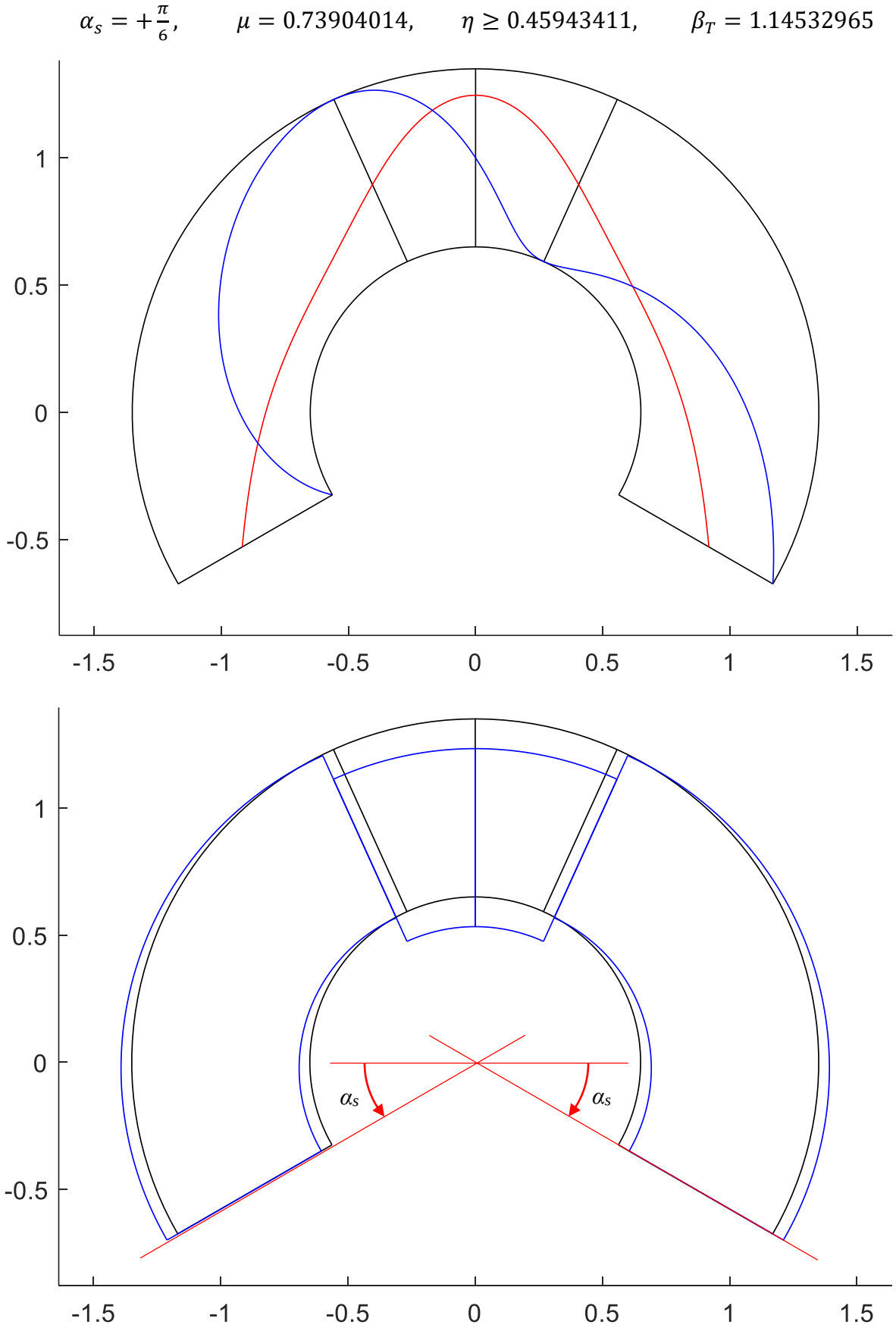

Figure 16: Characteristic values (top); lines of eccentricity (centre); collapse mechanism (bottom): purely sliding collapse.

$\alpha_s = 1, \qquad \mu \geq 2.3386589, \qquad \eta = 0.80543468, \qquad \beta_N = 0.67294349$

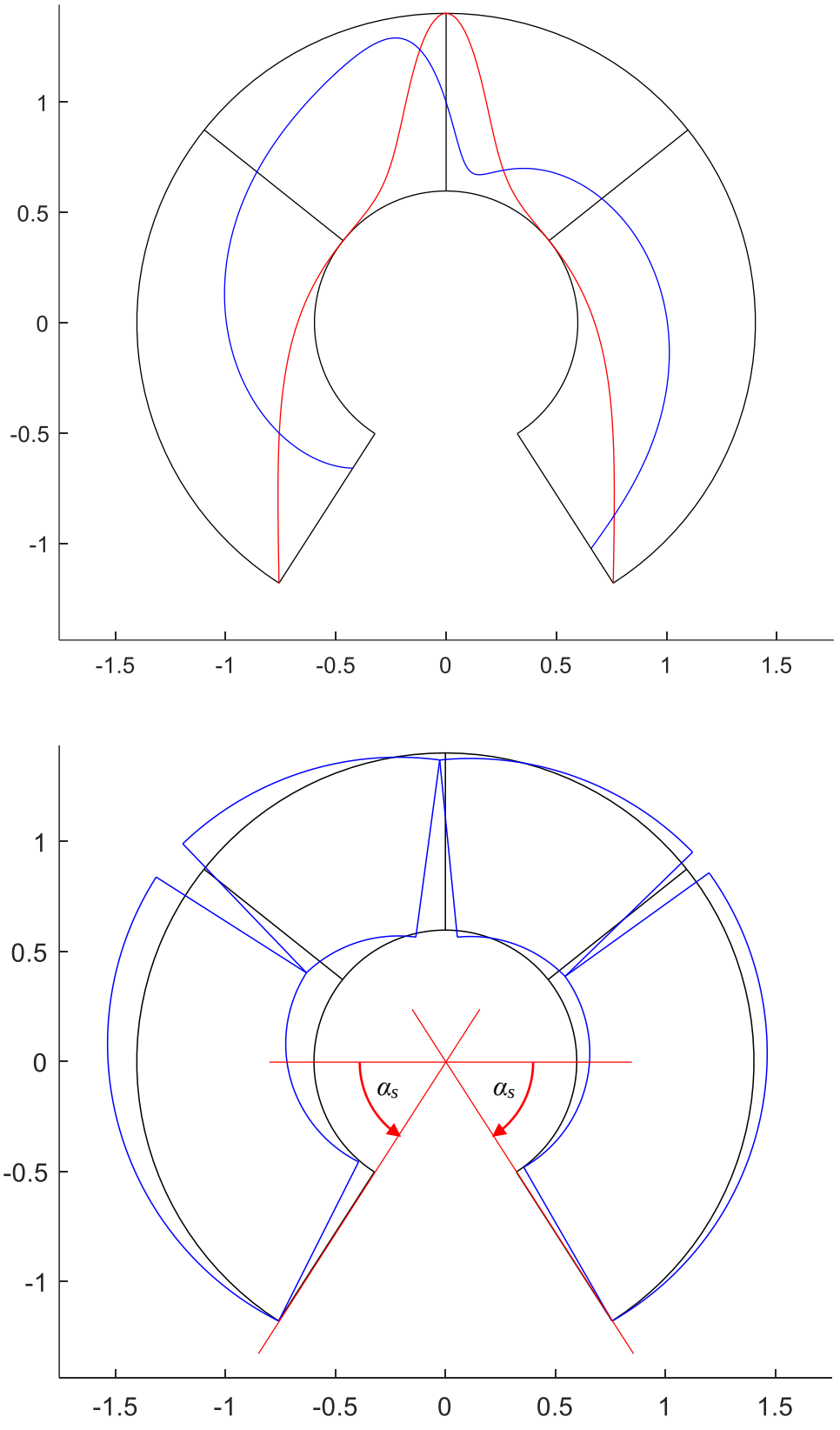

Figure 17: Characteristic values (top); lines of eccentricity (centre); collapse mechanism (bottom): purely rotational collapse.

$$\alpha_s = 1, \quad 1.6624129 \le \mu \le 2.3386589, \quad 0.86040507 \ge \eta \ge 0.80543468,$$
$$1.3070601 \le \beta_T \le 1.3716054, \quad 0.86910520 \ge \beta_N \ge 0.67294349$$

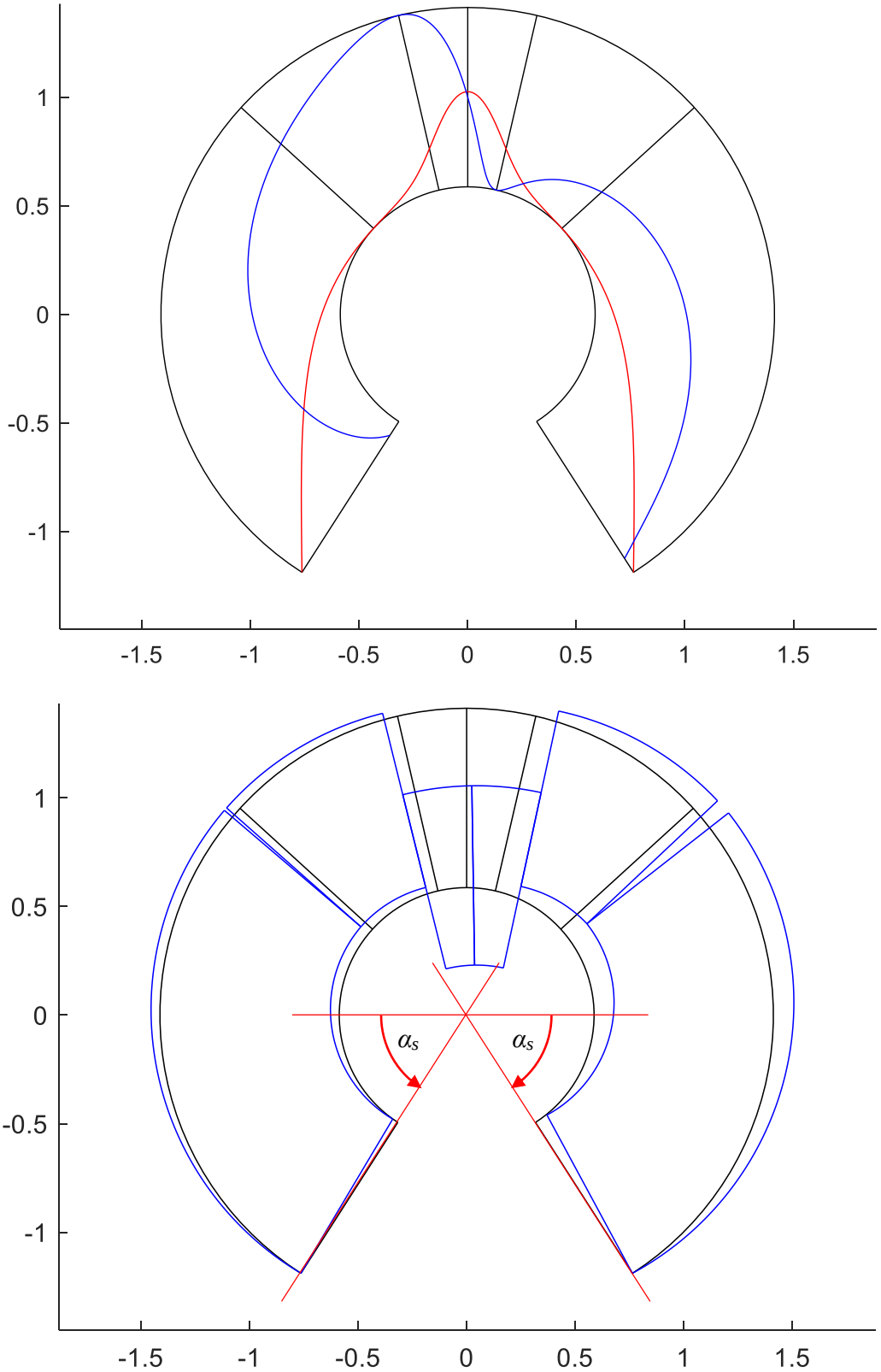

Figure 18: Characteristic values (top); lines of eccentricity (centre); collapse mechanism (bottom): mixed rotational–sliding collapse.

$\alpha_s = 1, \qquad \mu = 1.6624129, \qquad \eta \geq 0.86040507, \qquad \beta_T = 1.3070601$

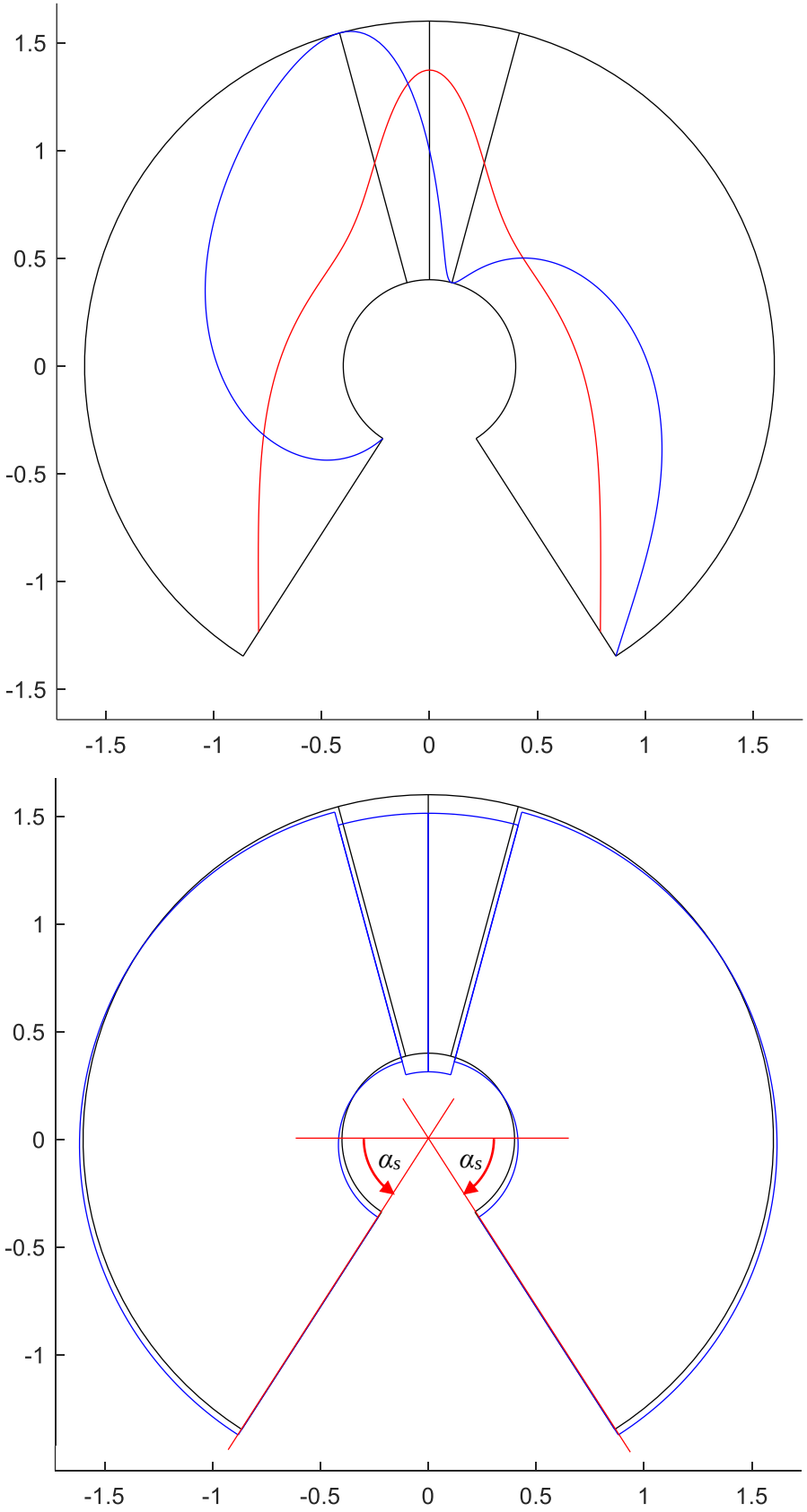

Figure 19: Characteristic values (top); lines of eccentricity (centre); collapse mechanism (bottom): purely sliding collapse.

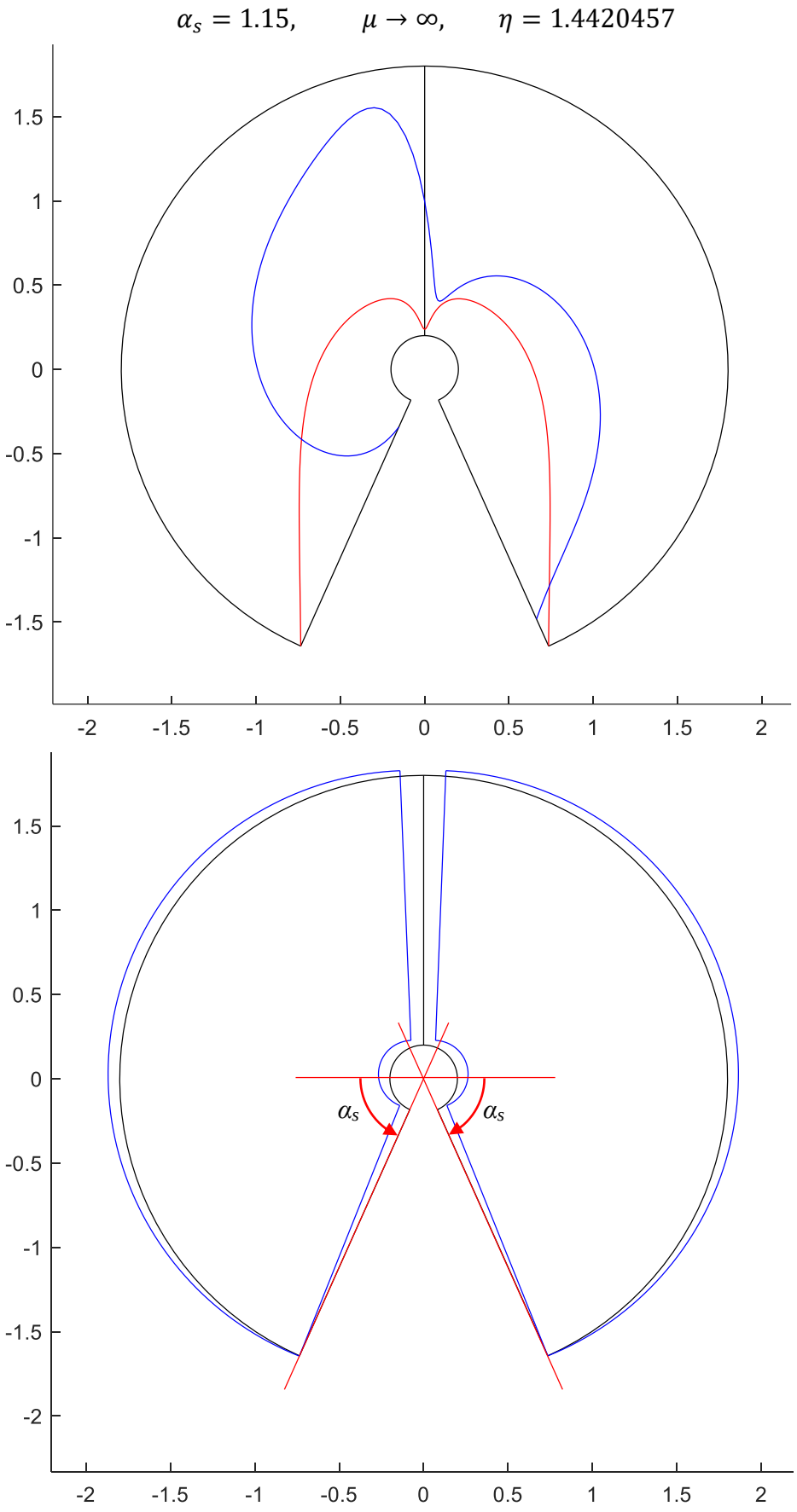

Figure 20: Characteristic values (top); lines of eccentricity (centre); collapse mechanism (bottom): overturning collapse.

$$\alpha_s = 1.15, \qquad 2.32956641 \leq \mu < \infty, \qquad 1.58035240 \geq \eta > 1.4420457,$$
$$1.37093086 \leq \beta_T < \pi/2$$

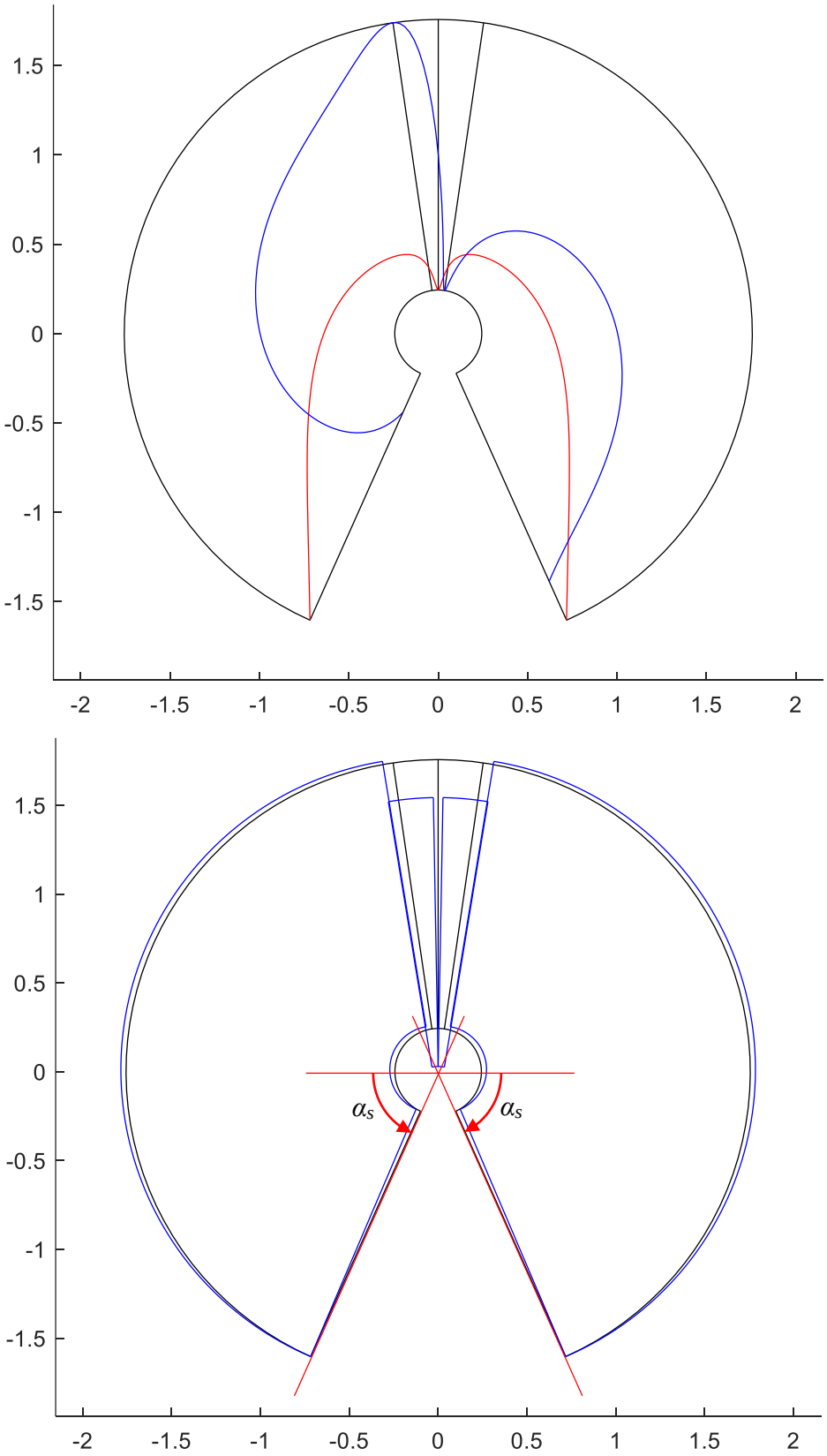

Figure 21: Characteristic values (top); lines of eccentricity (centre); collapse mechanism (bottom): mixed rotational–sliding collapse.

$\alpha_s = 1.15, \quad \mu = 2.32956641, \quad \eta = 1.58035240, \quad \beta_T = 1.37093086$

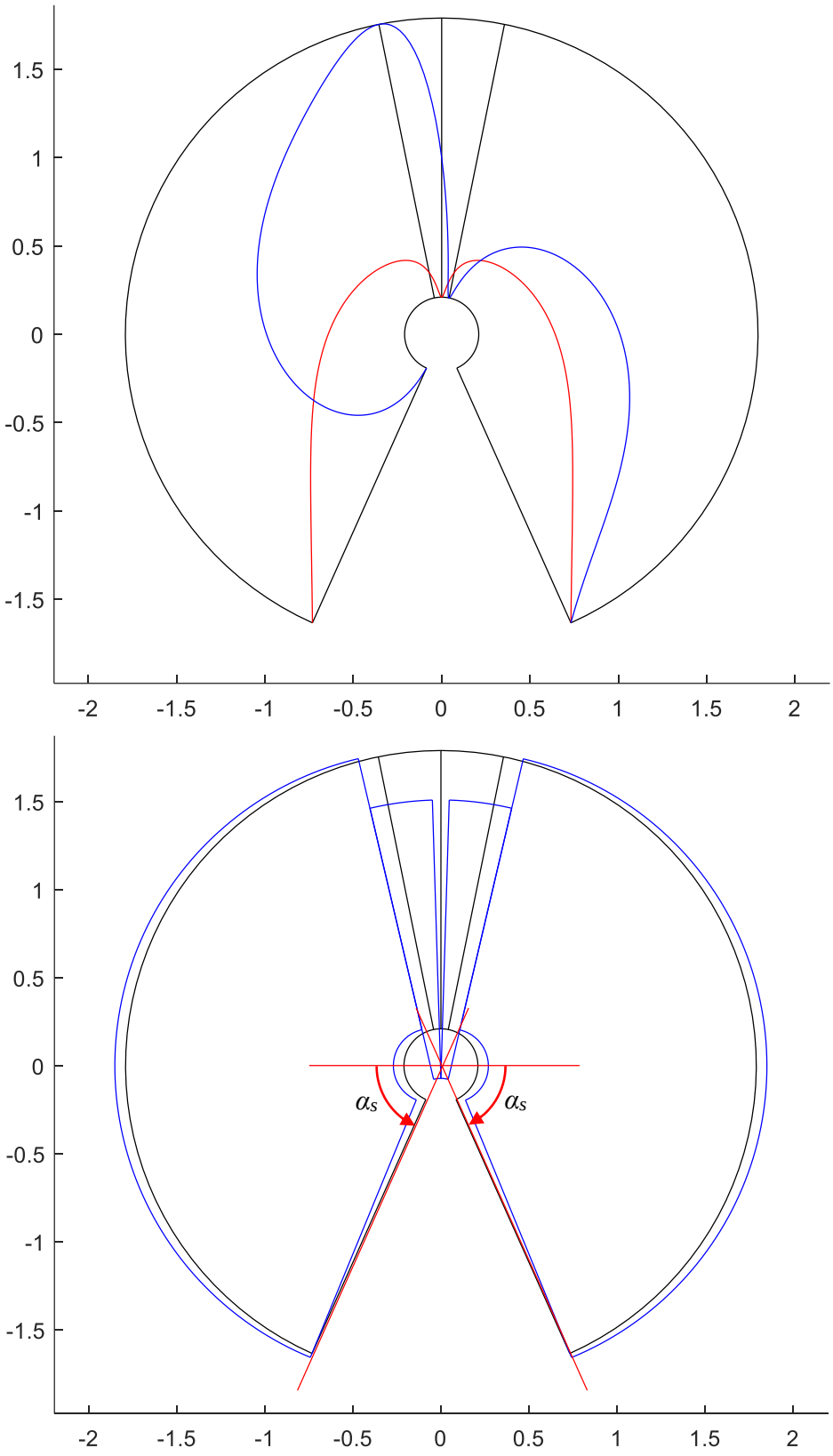

Figure 22: Characteristic values (top); lines of eccentricity (centre); collapse mechanism (bottom): mixed rotational–sliding collapse, with both rotation and sliding at the shoulders.

$\alpha_s = 1.15, \qquad \mu = 2.32956641, \qquad \eta \geq 1.58035240, \qquad \beta_T = 1.37093086$

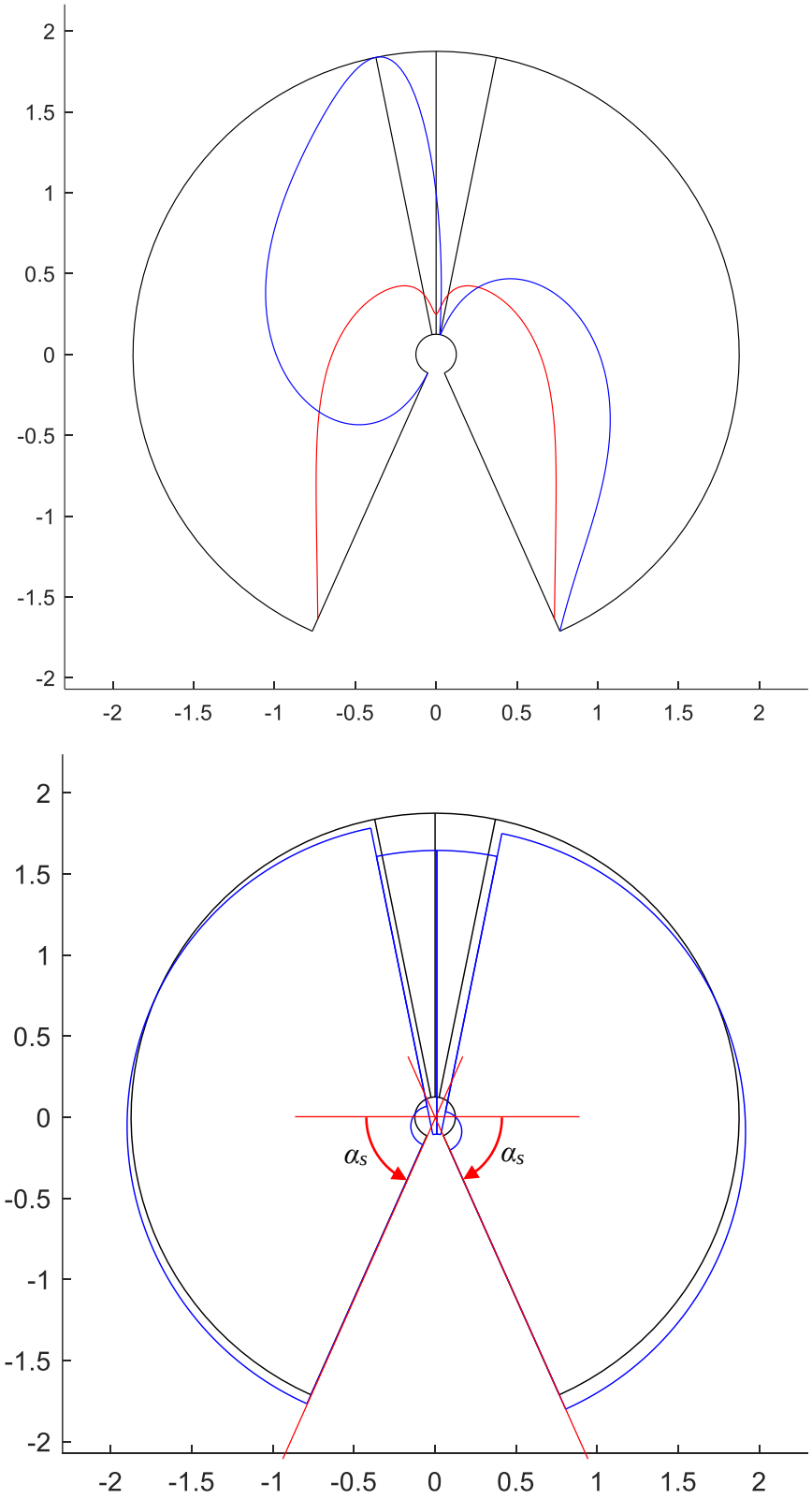

Figure 23: Characteristic values (top); lines of eccentricity (centre); collapse mechanism (bottom): purely sliding collapse.

Figure 24, together with Table 2, resumes the nomenclature and characteristic values of the specific parameters, for the considered values of symmetric arch openings. These sketches are typical piece–wise behaviours in the $\eta - \mu$ plane, as already pointed out in [18,21,23,34,36]. Results are academically provided with several (8) significative digits (even much beyond the number that may be meaningful for practical purposes), as they come out from the numerical procedure, to show the confirmed ability of the present novel numerical modelization. The range of friction coefficients in which mixed sliding–rotational collapse develops is recorded to be rather narrow, and may close down to zero.

This is further illustrated in Figs. 25–29, and in resuming Fig. 30. Figs. 25–29 truly show the iso–contours of optimization function $-\boldsymbol{\varphi}^T\boldsymbol{\lambda}$, out of the numerical process, and amazingly trace down the lower bound of the feasible states at its vanishing values, for the various considered values of arch openings. This fully testifies the validity and opportunity of the stated innovative numerical procedure based on non-linear programming.

Final Fig. 30 plays a conclusive core role and resumes the whole performed analyses, depicting the boundaries of the feasible states of the arch (limit equilibrium curves) in the η–μ plane, at variable α_s opening of the shoulder joint. Such boundaries are generated by numerically extracting the values leading to $-\boldsymbol{\varphi}^T\boldsymbol{\lambda} = 0$ after the optimization process. Transition (corner) points where there appears a change in the collapse mode (and where multiple collapse mechanisms become possible, by a linear combination of the mechanisms associated to the underlying branches merging at the common nodes) are marked, at reducing friction, with the corresponding arising values of least thickness of the self-standing masonry arch. It is worthwhile to remark that, for the analyzed circular symmetric masonry arches, uniqueness in the least thickness condition is still recovered, as earlier claimed in the literature (e.g. Casapulla and Lauro [35], Gilbert et al. [36]). The present formulation shall provide a sort of rigorous, though numerical, proof of such a uniqueness statement, for symmetric circular arches. Despite, the formulation shall be general enough to point out to potential different outcomes, with loss of uniqueness in least thickness, as they may come out for other instances of arch geometries (e.g. unsymmetric), as it may be inspected and analyzed separately.

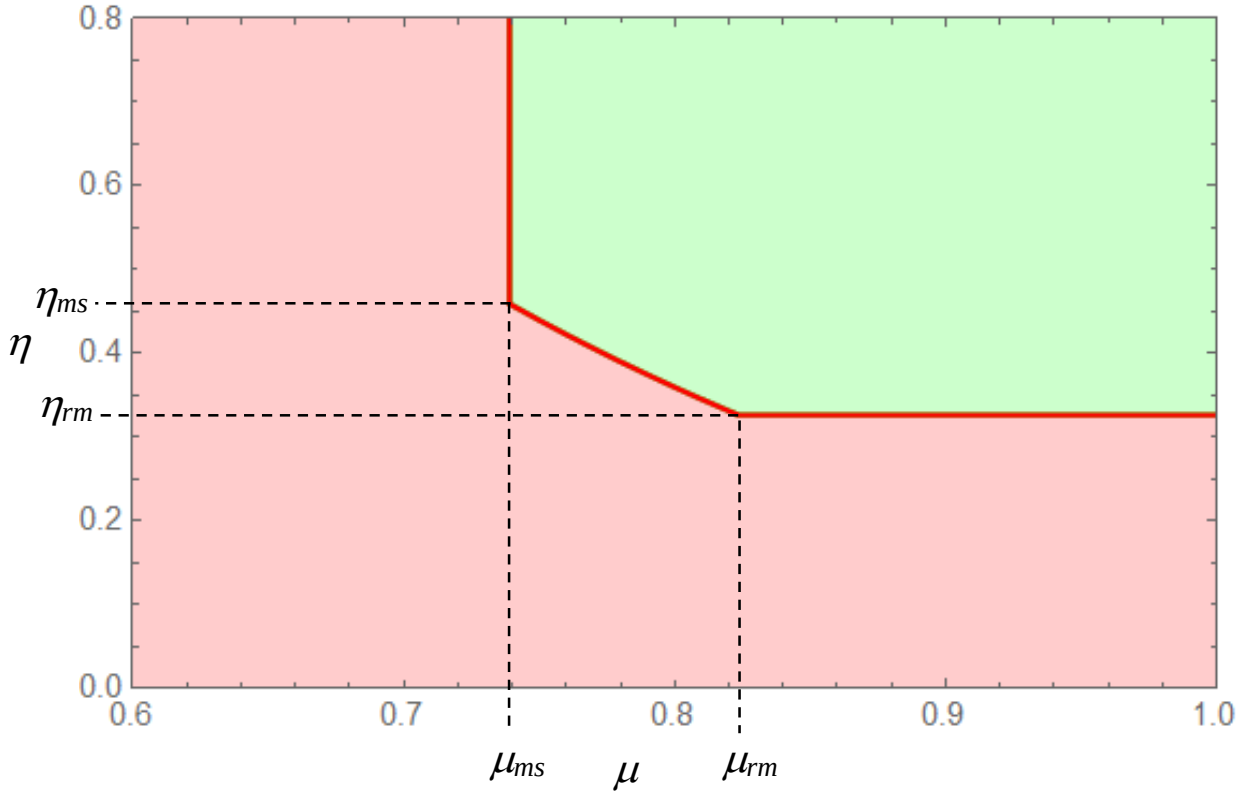

Figure 24: Nomenclature on limit−equilibrium curve separating the "safe domain" (upper, right) from the "collapse domain" (lower, left). Parameters have been indicated as coordinates of the corner points; refer to Table 2. Curve is here traced for $\alpha_s = \pi/6$.

α_s	μ_{ms}	ϕ_{ms}	η_{ms}	β_{Nms}	β_{Ts}
	μ_{rm}	ϕ_{rm}	η_{rm}	β_{Nrm}	–
[rad]	[–]	[deg]	[–]	[rad]	[rad]
$-\pi/6$	0.094375852	5.4	0.049002368	0.75740905	1.1343562
	0.14472273	8.2	0.022848202	0.88207486	–
0	0.30921544	17.2	0.20063732	0.51463788	1.0710004
	0.39583204	21.6	0.10742645	0.61965572	–
$\pi/6$	0.73904014	36.5	0.45943411	0.45365963	1.1453296
	0.82361489	39.5	0.32654664	0.44355547	–
1	1.6624129	59.0	0.86040507	0.86910520	1.3070601
	2.3386589	66.8	0.80543468	0.67294349	1.3716054
1.15	2.3295664	66.8	1.5803524	–	1.3709309
	∞	90.0	1.4420457	–	$\pi/2$

Table 2: Arch collapse characteristics at variable arch opening: critical friction coefficients and thickness to radius ratios (see nomenclature in Figure 24); angular position of opening and sliding joints.
Plots in Figures 8–23.

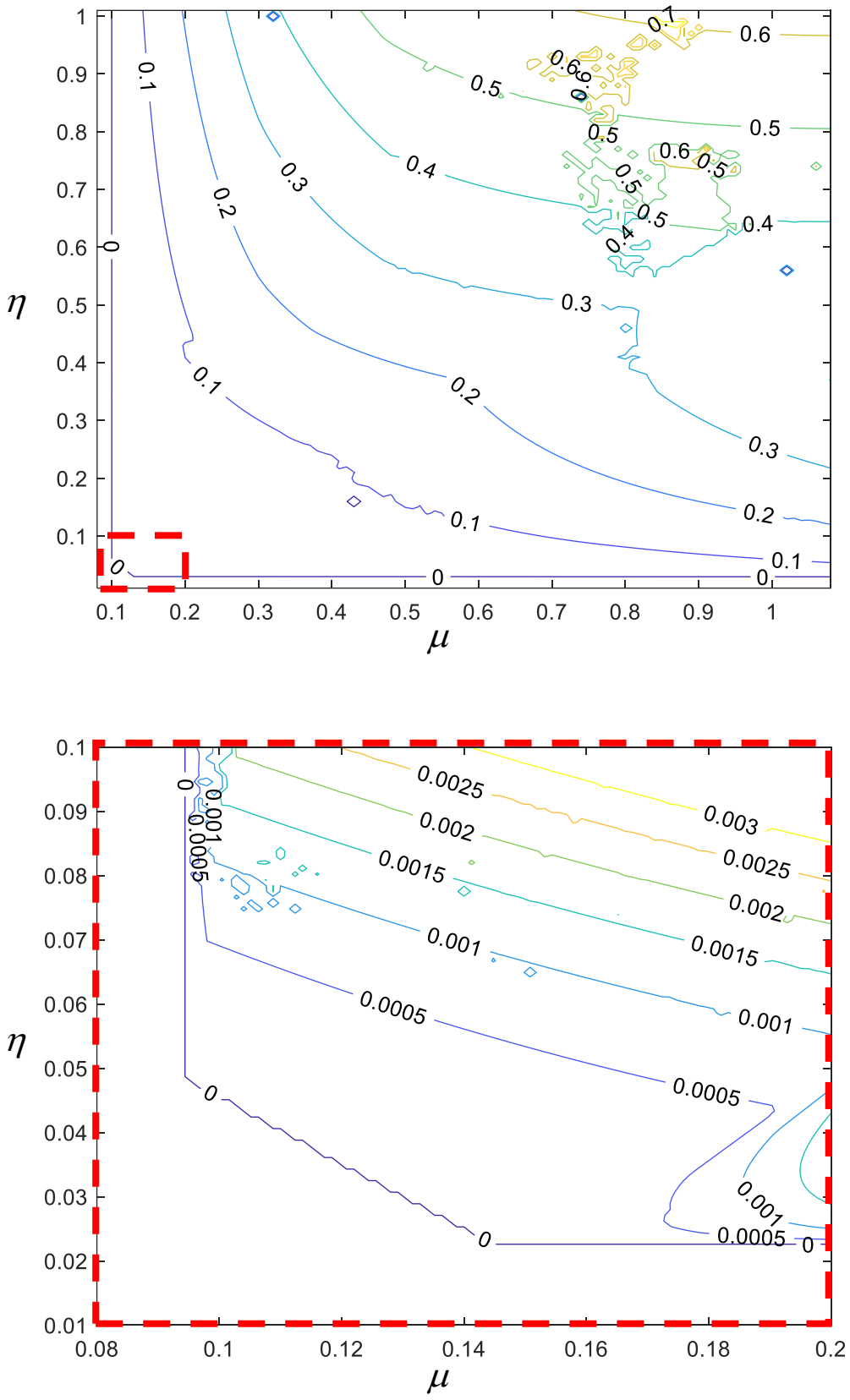

Figure 25: Numerical $-\boldsymbol{\varphi}^T\boldsymbol{\lambda}$ contour plot for $\alpha_s = -\pi/6$ (top), with zoom (below).

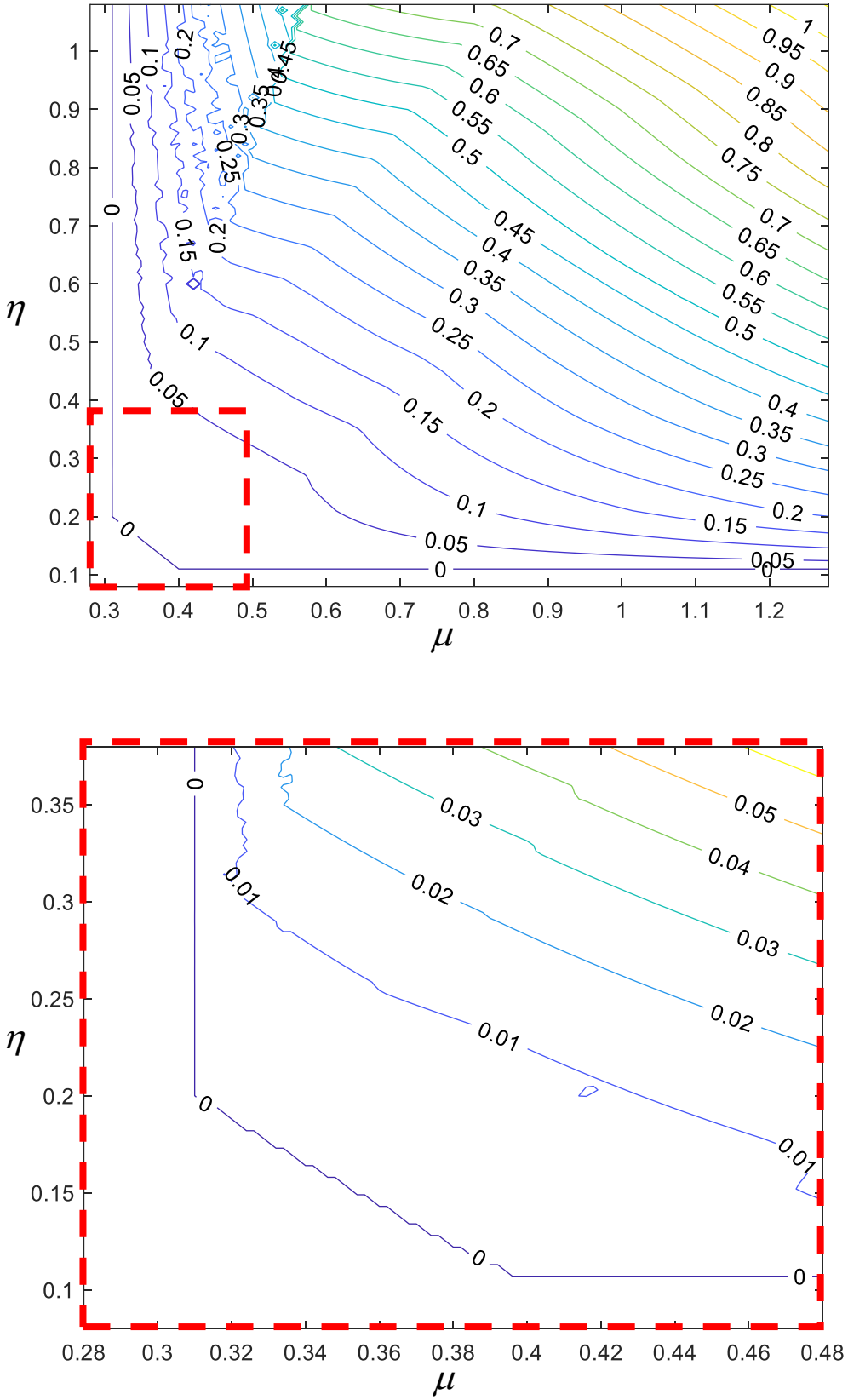

Figure 26: Numerical $-\boldsymbol{\varphi}^T\boldsymbol{\lambda}$ contour plot for $\alpha_s = 0$ (top), with zoom (below).

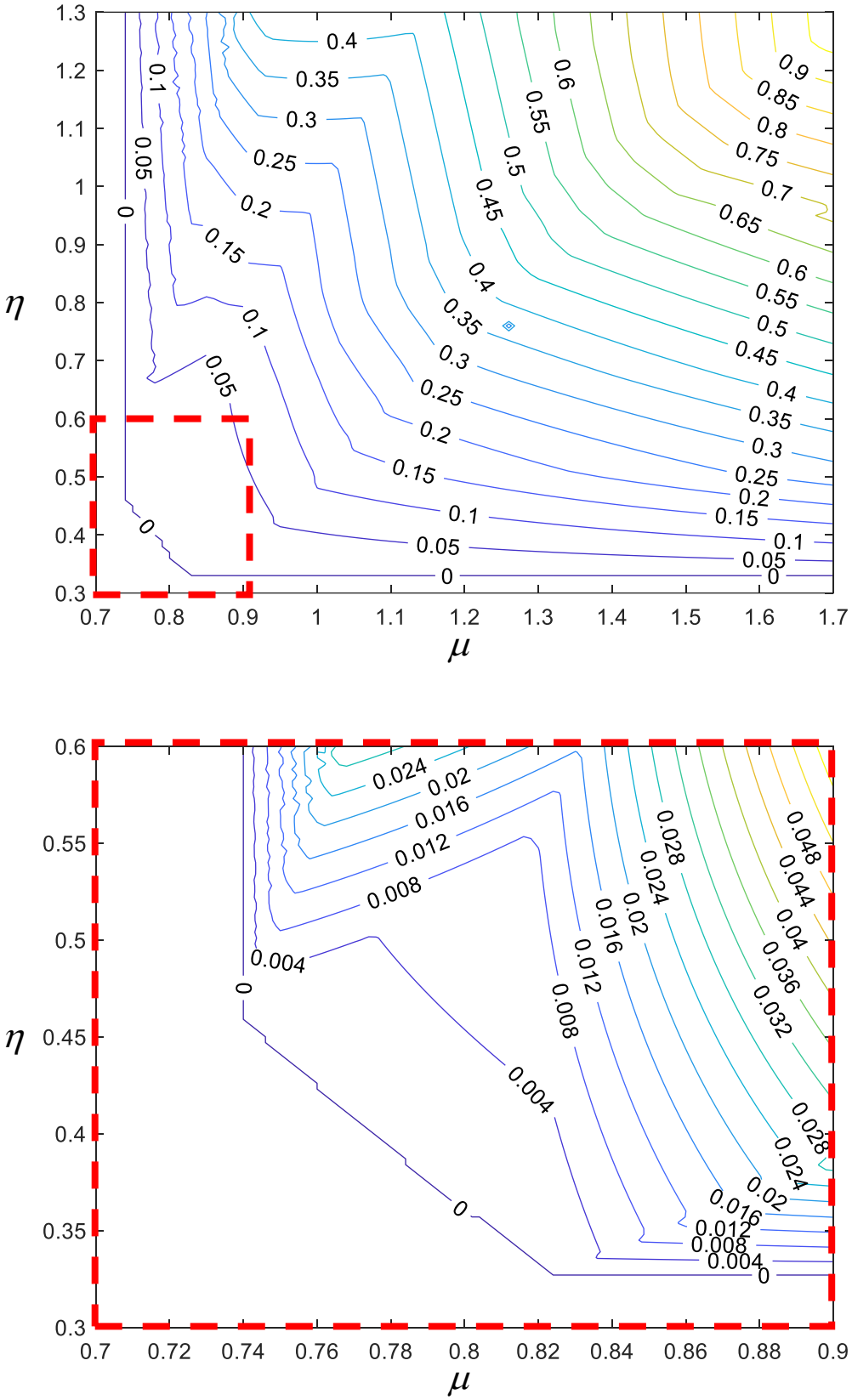

Figure 27: Numerical $-\boldsymbol{\varphi}^T\boldsymbol{\lambda}$ contour plot for $\alpha_s = +\pi/6$ (top), with zoom (below).

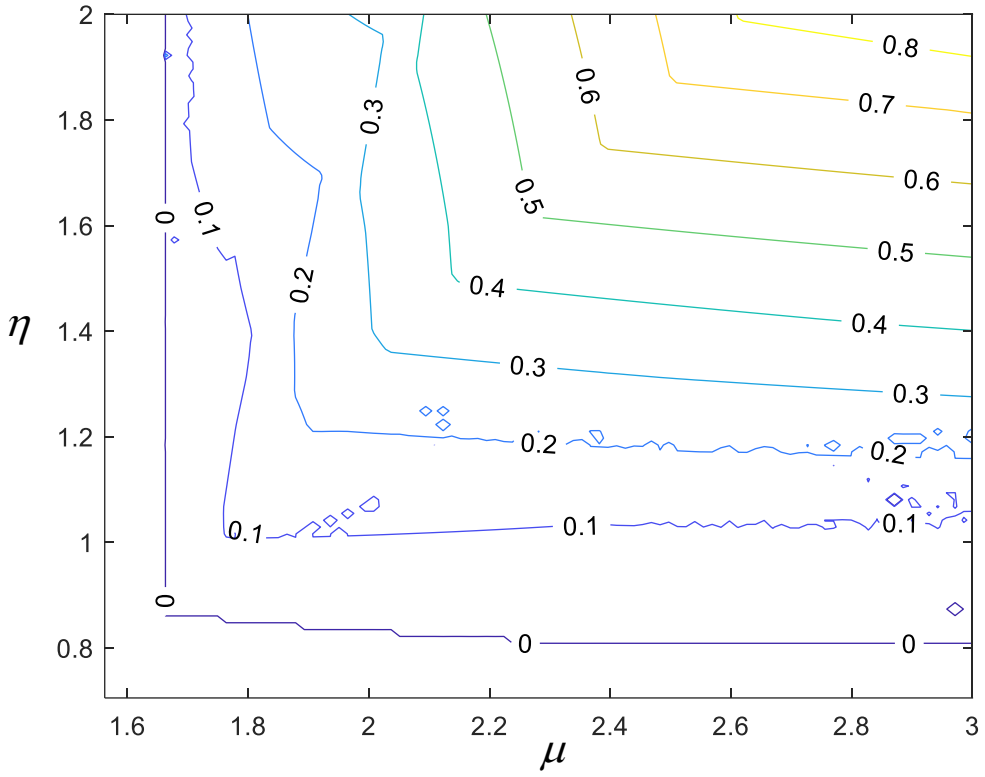

Figure 28: Numerical $-\boldsymbol{\varphi}^T\boldsymbol{\lambda}$ contour plot for α_s = 1.0.

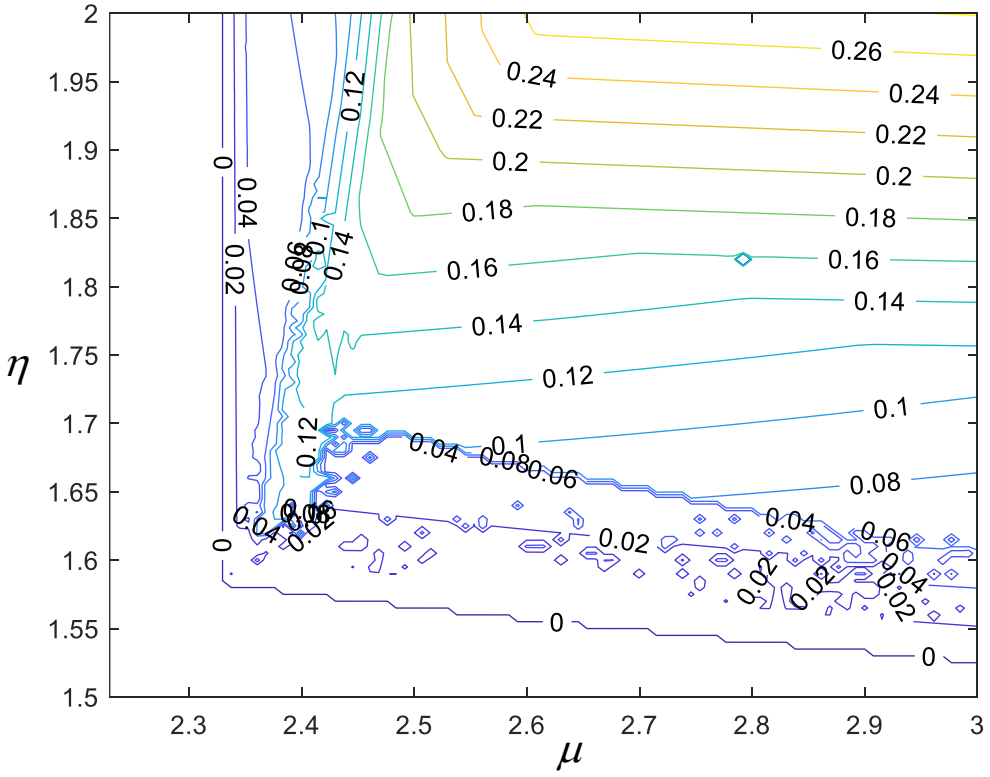

Figure 29: Numerical $-\boldsymbol{\varphi}^T\boldsymbol{\lambda}$ contour plot for α_s = 1.15.

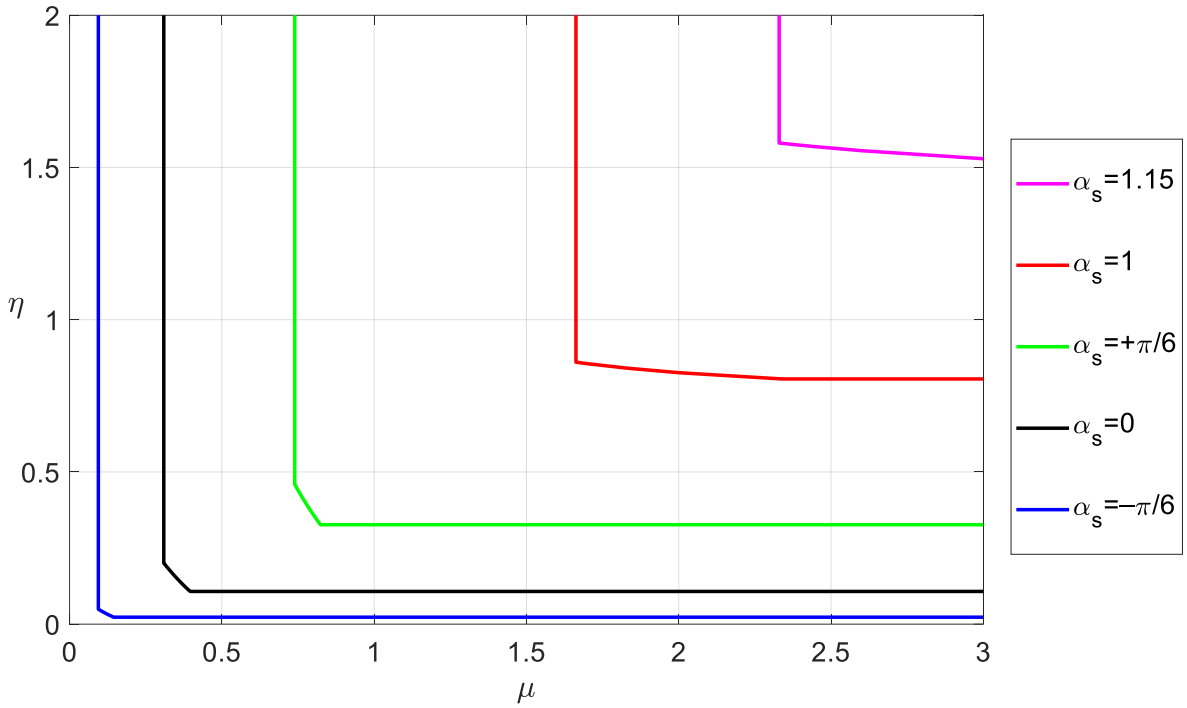

Figure 30: Limit equilibrium curves for considered opening angles α_s.

3.1 Computational remarks and technical considerations

In short, the computational strategies that have been developed to run the implemented procedure and lead to the obtained outcomes may be resumed as follows:

- About the definition of the (unknown) position of the failure joints, either rotational and/or sliding, few blocks have been initially defined (say, e.g., $n = 6$, with equally spaced radial joints along the arch); then, for given friction coefficient μ, thickness to radius ratio η is reduced down to get the tangency condition of the line of thrust, and/or the line of friction to the extrados and/or the intrados of the arch (i.e. the arch thickness is reduced until the stated problem becomes unfeasible). Finally, some of the joints are eliminated and the other ones are moved to the tangency points and, possibly, finely tuned to achieve an as high as needed precision for the numerical results. Notice that the need of devising an appropriate strategy to locate the failure joints, in an iterative process, spontaneously arises in the analyses of a continuous arch, and may be handled with different although seemingly similar procedures (see e.g. [28]).
- The left vertical branch of the feasible domain (e.g. the vertical edge at constant friction coefficient in Figure 24) is traced, for each given thickness, by reducing the friction coefficient down to the limiting value, below which an unfeasible solution is obtained. Three inner joints are initially assumed in free positions and a high friction coefficient is used; as a result, both the line of thrust and the line of friction lie within the arch thickness and $-\boldsymbol{\varphi}^T\dot{\boldsymbol{\lambda}} > 0$ corresponds to the optimal solution (i.e. a safe condition is obtained). Then, the progressive reduction of the friction coefficient brings to the tangency of the line of friction to the arch intrados and/or extrados; the inner joints are moved to such tangency points and, possibly, their position is tuned for the following (small) friction coefficient reduction, until limiting condition $-\boldsymbol{\varphi}^T\dot{\boldsymbol{\lambda}} = 0$ is reached (actually $\left|\hat{\boldsymbol{\varphi}}^T\hat{\dot{\boldsymbol{\lambda}}}\right| < 10^{-10}$, capped non–dimensional

variables being the original ones after appropriate normalization). Then, a further reduction of the friction coefficient yields to an unfeasible problem.

- The practical handling of the objective function within the minimization process and the dealing with the contour plots displayed in Figs. 25–29 have required the following strategies: a fine grid of evaluation points has been set in the $\eta-\mu$ plane, in the selected representative ranges; objective function $-\boldsymbol{\varphi}^T\dot{\boldsymbol{\lambda}}$ has been evaluated in such points; iso–contours are automatically generated by the built–in *contour* function in Matlab. Specifically, the handling of the lower bound of the $\eta-\mu$ limit condition for the mixed collapse mode at $-\boldsymbol{\varphi}^T\dot{\boldsymbol{\lambda}}=0$ has not been handled differently, but just accordingly to the same numerical interpolation strategy. This leads to the little waviness appearing in Figs. 25–29, as it comes out from the numerical computation (so, no attempt has been made to smoothen it, as it should be expected to appear, like sketched in Fig. 24).
- From the computation of the arch collapse characteristics to the graphical representation of the collapse modes, as reported in the above figures, the following aspects had to be considered: the value of the arch thickness is taken as the last value recorded before the problem becomes unfeasible, as stated in the first point above; kinematic mechanisms are plotted within a linear kinematics assumption, i.e. with displacements going like velocities; in some figures, the collapse could be obtained by a linear combination of more mechanisms: the represented ones have been taken as those simply delivered by the numerical algorithm, according to the numerical path truly followed within the optimization process.
    - Incidentally, this may lead to numerically derive, for symmetric arches, unsymmetric collapse mechanisms, as indeed testified by some of the instances depicted in the reported plots (see Figs. 12,13,17,18,23). This is also ruled by the underlying numerical solver that is adopted within the optimization procedure (see beginning of Section 3). Specifically, it has been obtained that the choice of the "i*nterior point*" vs. "a*ctive set*" method, in the optimization algorithm, generally leads to symmetric vs. non–symmetric mechanisms. Anyway, this is completely arbitrary. Indeed, notice that the collapse mode is by no mean imposed here to be symmetric, although the considered circular arch is symmetric; thus, being the number of effective degrees of freedom at least 2, for each mechanism, there is no reason, to generally expect, from the solution, a symmetric mechanism, and this not only for mechanisms involving sliding but also for purely rotational modes (see e.g. Fig. 17). Moreover, notice that the arrangement of rupture joints (either hinges or sliding joints) does fulfill symmetry, for symmetric arches, but the collapse mechanism, in general, shall not (even for purely rotational modes with hinges only or purely sliding ones with sliding joints only), since the collapse mechanism of the entire arch displays multiple dofs. Thus, the primary output of the present optimization algorithm, in the critical condition, is the reconstruction of the pattern of the rupture joints, as attached to the dislocations of the line of thrust and the line of friction. Such a pattern turns here out to be symmetric (as expected). The relevant collapse mode, though, is known unless for an arbitrary fixing of multiple residual degrees of freedom. It may be easy to be imposed that the collapse mode to be found and/or depicted be symmetric, but this is just one arbitrary choice. The kinematic solution comes from the implemented numerical process, and like that straight away plotted. The solution choice is tight to the numerical steps followed within the optimization procedure but is not a matter of numerical errors. In sum, one could state that the present formulation truly finds the (symmetric) position of the rupture joints. As it must be, the collapse mode is instead undefined (not uniquely defined), and what is plotted is just from one possible choice (of the residual dofs), the one

that right away comes from the real numerical solution that is derived by the implemented procedure.

The following technical considerations on the obtained outcomes on the statics of symmetric circular masonry arches at reducing friction are also in order:

- The numerical procedure turns out to be truly effective in locating all limit equilibrium states of the symmetric circular masonry arch and in quantifying the relevant collapse characteristics. This is worthwhile to be mentioned, since the procedure is quite general, and could then be adopted for other geometrical shapes of the masonry arch (for instance for "tilted" or unsymmetric ones) or for additional different morphological shapes (which shall require straight–forward adaptations in the analytical description devised in Section 2).
- The observed outcomes highlight a quite rich scenario of collapse features and all possible arch collapse regimes at reducing or, say, limited friction, even in the present somehow "constrained" examination context of symmetric arches. Although Heymanian purely rotational collapse may prevail at high (usually affordable) friction, variegated patterns may arise at reducing friction, which may be induced by several conditions, or linked to structural effects like loosening joints or settlements.
- It could be said that a value of friction coefficient higher than about 2.8 (friction coefficient angle higher than about 71°) in the sense of third Heyman hypothesis would prevent any form of sliding. The circular masonry arch looks as a consistent natural self–standing structural element, which highly relies, however, as several other examples in nature and human constructions, on the role of friction. A loosening of that may disrupt and dismantle the whole implant that is allowed by high friction.
- The present numerical procedure has been here adopted and explored with reference to the ideal solution of a continuous arch (as in the underlying "Couplet–Heyman" problem of finding the least–thickness condition). This leads to a necessary validation condition for the effectiveness of the numerical strategy. Once this is here assessed, the procedure could then be applied to realms where analytical or reference approaches and outcomes are not available, and also for specific given morphological locations and dispositions of discrete blocks, as built in a real constructed arch. In that, the agile procedure here developed shows great promise and expectation of application as a useful tool towards the safety analysis of masonry arches, becoming competing and/or alternative to other available formulations, as for instance classical Discrete Element Method (DEM) and other specific methods dedicated to the analysis of arches or vaulted masonry structures (see also extensive reference lists in [17] and [19]).

4 CONCLUSIONS

The present mathematical programming formulation of LA for circular masonry arches, in the presence of a limited friction, shows that an efficient numerical implementation has been achieved, for the analysis of the critical, least–thickness condition (incipient collapse) of symmetric circular masonry arches under self–weight, at variable friction coefficient. The numerical procedure truly allows to locate the critical characteristics of collapse of the arch at variable (reducing) friction coefficient.

Specifically, the limiting $\eta - \mu$ curve between critical thickness to radius ratio η and friction coefficient μ is effectively traced, separating the various collapse modes from the unfeasible states (i.e. those for which the arch cannot withstand its own self–weight). These can be

geometrically depicted, with a corresponding representation of the line of thrust and of the line of friction, e.g. of the eccentricities related to internal action ratios M/N and T/N.

Despite for the potential presence of non–normality effects of the flow rule, uniqueness of the collapse characteristics has been revealed, in terms of critical arch thickness, at any given supercritical friction coefficient still allowing the arch to withstand, in the analyzed cases of symmetric circular masonry arches, at least under the present condition of uniform self–weight distribution as a unique permanent loading. This looks consistent with what reported in previous literature contributions (see e.g. [35,36]).

Further generalizations of the present analysis may account for different types of external loading (for instance, by an independent horizontal action as a live load, affected by a load multiplier), in view of further exploring the existence of possible non–uniqueness ranges of the critical solutions in such a case. Same, also, for different types of masonry arch geometry or typology.

ACKNOWLEDGMENTS

This work has been carried–out at the University of Bergamo, Department of Engineering and Applied Sciences (Dalmine). The financial support by ministerial funds (MIUR) "*Fondi di Ricerca d'Ateneo ex 60%*" at the University of Bergamo is gratefully acknowledged.

REFERENCES

[1] J. Heyman, The stone skeleton. *International Journal of Solids and Structures*, **2**(2), 249–279, 1966. doi: 10.1016/0020-7683(66)90018-7.

[2] J. Heyman, On shell solutions for masonry domes. *International Journal of Solids and Structures*, **3**(2), 227–241, 1967. doi: 10.1016/0020-7683(67)90072-8.

[3] J.Heyman, The safety of masonry arches. *International Journal of Mechanical Sciences*, **11**(4), 363–385, 1969. doi: 10.1016/0020-7403(69)90070-8.

[4] J. Heyman, The Masonry Arch, Ellis Horwood Ltd., Chichester, 1982.

[5] M. Como, Equilibrium and collapse of masonry bodies. *Meccanica*, **27**(3), 185–194, 1992. doi: 10.1007/BF00430044.

[6] C. Blasi, P. Foraboschi, Analytical approach to collapse mechanisms of circular masonry arch. *Journal of Structural Engineering*, **120**(8), 2288–2309, 1994. doi: 10.1061/(ASCE)0733-9445(1994)120:8(2288).

[7] T.E. Boothby, Stability of masonry piers and arches including sliding. *Journal of Engineering Mechanics*, **120**(2), 304–319, 1994. doi: 10.1061/(ASCE)0733-9399(1994)120:2(304).

[8] M. Lucchesi, C. Padovani, G. Pasquinelli, N. Zani, On the collapse of masonry arches. *Meccanica*, **32**(4), 327–346, 1997. doi: 10.1023/A:1004275223879.

[9] F. Foce, Milankovitch's Theorie der Druckkurven: Good mechanics for masonry architecture. *Nexus Network Journal*, **9**(2), 185–210, 2007. doi: 10.1007/s00004-007-0039-9.

[10] J.A. Ochsendorf, Collapse of Masonry Structures. Ph.D. Thesis, University of Cambridge, King's College, UK, 2002.

[11] P. Block, M. DeJong, J. Ochsendorf, As hangs the flexible line: Equilibrium of masonry arches. *Nexus Network Journal*, **8**(2), 13–24, 2006. doi: 10.1007/s00004-006-0015-9.

[12] J.A. Ochsendorf, The masonry arch on spreading supports. *Structural Engineer*, **84**(2), 29–35, 2006.

[13] A. Romano, J.A. Ochsendorf, The mechanics of Gothic masonry arches. *International Journal of Architectural Heritage*, **4**(1), 59–82, 2010. doi: 10.1080/15583050902914660.

[14] A.S. Gago, Análise Estrutural de Arcos, Abóbadas e Cúpulas – Contributo para o Estudo do Património Construído, Dissertação, Doutoramento em Engenharia Civil, Orientador: A. Lamas, Universidade Técnica de Lisboa, Instituto Superior Técnico, IST–UTL, Dezembro de 2004.

[15] A.S. Gago, J. Alfaiate, A. Lamas, The effect of the infill in arched structures: Analytical and numerical modelling. *Engineering Structures*, **33**(5), 1450–1458, 2011. doi: 10.1016/j.engstruct.2010.12.037.

[16] E. Rizzi, G. Cocchetti, G. Colasante, F. Rusconi, Analytical and numerical analysis on the collapse mode of circular masonry arches. *Advanced Materials Research* (ISSN: 1662-8985), **133**–**134**, 467–472, 2010. doi: 10.4028/www.scientific.net/AMR.133-134.467.

[17] G. Cocchetti, G. Colasante, E. Rizzi, On the analysis of minimum thickness in circular masonry arches. *Applied Mechanics Reviews*, **64**(5), 1–27, 2012. doi:10.1115/1.400747.

[18] E. Rizzi, G. Colasante, A. Frigerio, G. Cocchetti, On the mixed collapse mechanism of semi–circular masonry arches. *Proc. 8th Int. Conf. on Structural Analysis of Historical Constructions (SAHC 2012)*, J. Jasienko ed., Wroclaw, Poland, 15–17 October 2012, Vol. 1, 541–549. ISSN 0860-2395, ISBN: 978-83-7125-216-7, 2012. Also available at www.hms.civil.uminho.pt/sahc/.

[19] E. Rizzi, F. Rusconi, G. Cocchetti, Analytical and numerical DDA analysis on the collapse mode of circular masonry arches. *Engineering Structures*, **60**(February 2014), 241–257, 2014. doi: 10.1016/j.engstruct.2013.12.023.

[20] G. Cocchetti, E. Rizzi, Limit analysis of circular masonry arches at reducing friction, *Proc. 10th International Masonry Conference (10th IMC)*, G. Milani, A. Taliercio, S. Garrity eds., Milan, Italy, 9–11 July 2018, USB Proceedings, 486–503, 2018.

[21] G. Cocchetti, E. Rizzi, Analytical and numerical analysis on the collapse modes of least-thickness circular masonry arches at decreasing friction. Submitted for publication, revised version, 2019.

[22] D. Aita, R. Barsotti, S. Bennati, Equilibrium of pointed, circular, and elliptical masonry arches bearing vertical walls. *Journal of Structural Engineering*, **138**(7), 880–888, 2012. doi: 10.1061/(ASCE)ST.1943-541X.0000522.

[23] D. Aita, R. Barsotti, S. Bennati, Looking at the collapse modes of circular and pointed masonry arches through the lens of Durand–Claye's stability area method. *Archive of Applied Mechanics*, 1–18, 2019. doi: 10.1007/s00419-019-01526-z.

[24] H. Alexakis, N. Makris, Minimum thickness of elliptical masonry arches. *Acta Mechanica*, **224**(12), 2977–2991, 2013. doi: 10.1007/s00707-013-0906-2.

[25] N. Makris, H. Alexakis, The effect of stereotomy on the shape of the thrust–line and the minimum thickness of semicircular masonry arches. *Archive of Applied Mechanics*, **83**(10), 1511–1533, 2013. doi: 10.1007/s00419-013-0763-4.

[26] H. Alexakis, N. Makris, Limit equilibrium analysis of masonry arches. *Archive of Applied Mechanics*, **85**(9–10), 1363–1381, 2015. doi: 10.1007/s00419-014-0963-6.

[27] N. Cavalagli, V. Gusella, L. Severini, Lateral loads carrying capacity and minimum thickness of circular and pointed masonry arches. *International Journal of Mechanical Sciences*, **115**–**116**(September 2016), 645–656, 2016. doi: 10.1016/j.ijmecsci.2016.07.015.

[28] D. Nikolić, Thrust line analysis and the minimum thickness of pointed masonry arches. *Acta Mechanica*, **228**(6), 2219–2236, 2017. doi: 10.1007/s00707-017-1823-6.

[29] M. Angelillo, The model of Heyman and the statical and kinematical problems for masonry structures. *International Journal of Masonry Research and Innovation*, **4**(1–2), 14–31, 2019. doi: 10.1504/IJMRI.2019.096820.

[30] O. Gáspár, A.A. Sipos, I. Sajtos, Effect of stereotomy on the lower bound value of minimum thickness of semi–circular masonry arches. *International Journal of Architectural Heritage*, **12**(6), 899–921, 2018. doi: 10.1080/15583058.2017.1422572.

[31] K. Bagi, When Heyman's Safe Theorem of rigid block systems fails: Non–Heymanian collapse modes of masonry structures. *International Journal of Solids and Structures*, **51**(14), 2696–2705, 2014. doi: 10.1016/j.ijsolstr.2014.03.041.

[32] G.Lengyel, Minimum thickness of the gothic arch. *Archive of Applied Mechanics*, **88**(5), 769–788, 2018. doi: 10.1007/s00419-018-1341-6.

[33] N.M. Auciello, On the analysis of masonry arches. *International Journal of Masonry Research and Innovation*, **4**(1–2), 50–63, 2019. doi: 10.1504/IJMRI.2019.096821.

[34] A. Sinopoli, M. Corradi, F. Foce. Modern formulation for preelastic theories on masonry arches. *Journal of Engineering Mechanics*, **123**(3), 204–213, 1997. doi: 10.1061/(ASCE)0733-9399(1997)123:3(204).

[35] C. Casapulla, F. Lauro, A simple computation tool for the limit–state analysis of masonry arches. *Proc. of 5th Int. Congress on Restoration of Architectural Heritage*, Università di Firenze, 17–24 September 2000, CDROM Proc., pp. 2056–2064, 9 pages, 2000.

[36] M. Gilbert, C. Casapulla, H.M. Ahmed, Limit analysis of masonry block structures with non–associative frictional joints using linear programming. *Computers and Structures*, **84**(13–14), 873–887, 2006. doi: 10.1016/j.compstruc.2006.02.005.

[37] C. Casapulla, D. D'Ayala, Lower bound approach to the limit analysis of 3D vaulted block masonry structures. *Proc. of the 5th Int. Symposium on Computer Methods in Structural Masonry, STRUMAS V*, Roma, pp. 28–36, Swansea, Computer and Geotechnics Ltd., 2001.

[38] D. D'Ayala, C. Casapulla, Limit state analysis of hemisferical domes with finite friction, in "Historical Constructions 2001 – Possibilities of Numerical and Experimental Techniques". *Proc. of the 3rd Int. Seminar*, P.B. Lourenço and P. Roca (Eds.), Guimarães, Portugal, University of Minho, Art. 056, pp. 617–626, 7–8–9 November 2001, 2001.

[39] D. D'Ayala, E. Tomasoni, Three–dimensional analysis of masonry vaults using limit state analysis with finite friction. *International Journal of Architectural Heritage*, **5**(2), 140–171, 2011. doi: 10.1080/15583050903367595.

[40] P. Smars. Etudes sur la stabilité des arcs et voûtes: Confrontation des méthodes de l'analyse limite aux voûtes gothique en Brabant, Doctoral Thesis, Katholieke Universiteit Leuven, Belgium, 229 pages, 2000.

[41] P. Smars. Influence of friction and tensile resistance on the stability of masonry arches. *Structural Analysis of Historic Construction: Preserving Safety and Significance – Proceedings of the 6th International Conference on Structural Analysis of Historic Construction (SAHC 2008)*, D. D'Ayala and E. Fodde eds., Bath (UK), Volume 2, pp. 1199–1206, Taylor & Francis Group, London, 2–4 July 2008. ISBN: 0415468728; 978-041546872-5, 2008.

[42] P. Smars, Kinematic stability of masonry arches. *Advanced Materials Research*, **133**–**134**, 429–434, 2010. doi: 10.4028/www.scientific.net/AMR.133-134.429.

[43] R.S. Olivito, M. Esposito, N. Totaro, Experimental investigation for the friction evaluation in the masonry structures. *International Journal of Masonry Research and Innovation*, **1**, 22–47, 2016. doi: 10.1504/IJMRI.2016.074729.

[44] F. Portioli, C. Casapulla, M. Gilbert, L. Cascini, Limit analysis of 3D masonry block structures with non–associative frictional joints using cone programming. *Computers and Structures*, **143**(September 2014), 108–121, 2014. doi: 10.1016/j.compstruc.2014.07.010.

[45] L. Cascini, F. Portioli, R. Landolfo, 3D rigid block micro–modelling of a full–scale unreinforced brick masonry building using mathematical programming. *International Journal of Masonry Research and Innovation*, **1**, 189–206, 2016. doi: 10.1504/IJMRI.2016.080426.

[46] G. Milani, A. Tralli, A simple meso–macro model based on SQP for the non–linear analysis of masonry double curvature structures. *International Journal of Solids and Structures*, **49**(5), 808–834, 2012. doi: 10.1016/j.ijsolstr.2011.12.001.

[47] E. Sacco, Stress approaches for the analysis of masonry arches. *Proc. 8th Int. Conf. on Structural Analysis of Historical Constructions (SAHC 2012)*, J. Jasienko ed., Wroclaw, Poland, 15–17 October 2012, Vol. 1, 550–558. ISSN 0860-2395, ISBN: 978-83-7125-216-7, 2012.

[48] C. Baggio, P. Trovalusci, Collapse behaviour of three-dimensional brick–block systems using non–linear programming. *Structural Engineering and Mechanics*, **10**(2), 181-195, 2000. doi: 10.12989/sem.2000.10.2.181.

[49] V. Beatini, G. Royer–Carfagni, A. Tasora, A regularized non–smooth contact dynamics approach for architectural masonry structures, *Computers and Structures*, **187**(15 July 2017), 88–100, 2017. doi: 10.1016/j.compstruc.2017.02.002.

[50] V. Beatini, G. Royer–Carfagni, A. Tasora, Modeling the shear failure of segmental arches. *International Journal of Solids and Structures*, **158**(February 2019), 21–39, 2019. doi: 10.1016/j.ijsolstr.2018.08.023.

[51] M. Angelillo, A. Fortunato, A. Gesualdo, A. Iannuzzo, G. Zuccaro, Rigid block models for masonry structures. *International Journal of Masonry Research and Innovation*, **3**(4), 2018. doi: 10.1504/IJMRI.2018.095701.

[52] G. Tempesta, S. Galassi, Safety evaluation of masonry arches. A numerical procedure based on the thrust line closest to the geometrical axis. *International Journal of Mechanical Sciences*, **155**(May 2019), 206–221, 2019. doi: 10.1016/j.ijmecsci.2019.02.036.

[53] F. Trentadue, G. Quaranta, Limit analysis of frictional block assemblies by means of fictitious associative−type contact interface laws. *International Journal of Mechanical Sciences*, **70**(May 2013), 140–145, 2013. doi: 10.1016/j.ijmecsci.2013.02.012.

[54] M.C. Ferris, F. Tin−Loi, Limit analysis of frictional block assemblies as a mathematical program with complementarity constraints. *International Journal of Mechanical Sciences*, **43**(1), 209−224, 2001. doi: 10.1016/S0020-7403(99)00111-3.

[55] A.R.S. Ponter, Shakedown limit theorems for frictional contact on a linear elastic body. *European Journal of Mechanics A/Solids*, **60**(November−December 2016), 17−27, 2016. doi: 10.1016/j.euromechsol.2016.05.003.

[56] J. Simon, K. Bagi, Discrete element analysis of the minimum thickness of oval masonry domes. *International Journal of Architectural Heritage*, **10**(4), 457−475, 2016. doi: 10.1080/15583058.2014.996921.

[57] F.C. Figueiredo, L.A. Borges, Limit analysis formulation for frictional problems. *Archive of Applied Mechanics*, **87**(12), 1965−1977, 2017. doi: 10.1007/s00419-017-1304-3.

[58] G. Maier, A minimum principle for incremental elastoplasticity with non−associated flow laws. *Journal of the Mechanics and Physics of Solids*, **18**(5), 319−330, 1970. doi: 10.1016/0022-5096(70)90002-5.

[59] G. Bolzon, G. Cocchetti, On a case of crack path bifurcation in cohesive materials. *Archive of Applied Mechanics*, **68**(7−8), 513−523, 1998. doi: 10.1007/s004190050183.

[60] G. Bolzon, G. Cocchetti, Direct assessment of structural resistance against pressurized fracture, *International Journal for Numerical and Analytical Methods in Geomechanics*, **27**(5), 353−378, 2003. doi: 10.1002/nag.276.

[61] G. Cocchetti, G. Maier, Elastic−plastic and limit−state analyses of frames with softening plastic−hinge models by mathematical programming. *International Journal of Solids and Structures*, **40**(25), 7219−7244, 2003. doi: 10.1016/S0020-7683(03)00363-9.

[62] G. Bolzon, Complementarity problems in structural engineering: an overview. *Archives of Computational Methods in Engineering*, **24**(1), 23−36, 2017. doi: 10.1007/s11831-015-9158-8.

[63] R. Ferrari, G. Cocchetti, E. Rizzi, Elastoplastic structural analysis of the Paderno d'Adda bridge (Italy, 1889) based on Limit Analysis, *Proc. of 8th International Conference on Structural Analysis of Historical Constructions (SAHC 2012)*, J. Jasienko ed., Wroclaw, Poland, Volume 3, pp. 2171−2180, DWE, Wroclaw, Poland, 15−17 October 2012, ISSN: 0860-2395, ISBN: 978-83-7125-216-7, 2012. Also available at www.hms.civil.uminho.pt/sahc/.

[64] R. Ferrari, G. Cocchetti, E. Rizzi, Limit analysis of a historical iron arch bridge. Formulation and computational implementation. *Computers and Structures*, **175**(15 October 2016), 184–196, 2016. doi: 10.1016/j.compstruc.2016.05.007.

[65] R. Ferrari, G. Cocchetti, E. Rizzi, Computational elastoplastic limit analysis of the Paderno d'Adda bridge (Italy, 1889). *Archives of Civil and Mechanical Engineering*, **18**(1), 291–310, 2018. doi: 10.1016/j.acme.2017.05.002.

[66] R. Ferrari, G. Cocchetti, E. Rizzi, Effective iterative algorithm for the Limit Analysis of truss–frame structures by a kinematic approach. *Computers and Structures*, **197**(15 February 2018), 28–41, 2018. doi: 10.1016/j.compstruc.2017.11.018.

[67] R. Ferrari, G. Cocchetti, E. Rizzi, Reference structural investigation on a 19th–century arch iron bridge loyal to design–stage conditions. *International Journal of Architectural Heritage*, Published online: 05 July 2019. doi: 10.1080/15583058.2019.1613453.

[68] R. Ferrari, G. Cocchetti, E. Rizzi, Evolutive and kinematic Limit Analysis algorithms for large-scale 3D truss-frame structures: comparison application to historic iron bridge arch. *International Journal of Computational Methods*, accepted for publication, doi: 10.1142/S0219876219400206, 2019.

[69] R.W. Cottle, J.S. Pang, R.E. Stone, The Linear Complementarity Problem. Academic Press, San Diego, 1992.

[70] Z.Q. Luo, J.S. Pang, D. Ralph, Mathematical Programs with Equilibrium Constraints, Cambridge University Press, 1996.

[71] E.S. Mistakidis, G.E. Stavroulakis, Nonconvex Optimization in Mechanics, Kluwer Academic Publishers, 1998.

[72] F. Facchinei, H. Jiang, L. Qi, A smoothing method for mathematical programs with equilibrium constraints. *Mathematical Programming*, **85**(1), 107–134, 1999. doi: 10.1007/s10107990015a.

[73] D.Y. Gao, R.W. Ogden, G.E. Stavroulakis (Eds.), Nonsmooth/Nonconvex Mechanics, Kluwer Academic Publishers, 2001.